Land Use Policy 174 (2027) 108431

Contents lists available at ScienceDirect

Land Use Policy

journal homepage: www.elsevier.com/locate/landusepol

A transferable framework for integrating shared socioeconomic pathways into hybrid urban growth models: Lessons from central Vietnam

Olabisi S. Badmos [a,b,*], Oluwafemi M. Odunsi [c], Andrea Ortiz Vargas [d], Bien Thanh Vu [a], Lena C. Grobusch [a,e], Antje Katzschner [a], Linh Nguyen Hoang Khanh [f], Volker Hochschild [g], Felix Bachofer [h], Matthias Garschagen [a,b]

[a] Human Environment Relations (HER), Department of Geography, Ludwig-Maximilians-Universität, München, Luisenstr. 37, Munich 80333, Germany
[b] Development of Urban and Rural Regions, Institute of Geodesy and Geoinformation (IGG), University of Bonn, Nußallee 1, Bonn 53115, Germany
[c] Interdisciplinary Geoinformation Sciences, Institute of Geography, Ruhr-Universität Bochum, Universitätsstr. 150, Bochum 44801, Germany
[d] United Nations University, Institute for Environment and Human Security (UNU-EHS), Bonn, Germany
[e] Climate-KIC, Plantage Middenlaan 45, Amsterdam 1018 DC, the Netherlands
[f] International School, Hue University, Hue City 0234, Viet Nam
[g] Department of Geosciences, Institute of Geography, University of Tübingen, Tübingen 72070, Germany
[h] DLR German Aerospace Center (DLR)—Earth Observation Center (EOC), Wessling, Germany

ARTICLE INFO

Keywords:
Shared socioeconomic pathway
Cellular automata
Land-use change
Sustainable urban development
Scenario downscaling

ABSTRACT

Translating global Shared Socioeconomic Pathways (SSPs) into locally grounded, spatially explicit urban scenarios remains a methodological challenge for urban futures research. This study develops a hybrid framework that combines participatory SSP downscaling, Random Forest-derived urban growth propensity, scenario specific spatial protection, and stochastic cellular automata simulation to examine alternative urban futures for Hue, Vietnam, to 2050. Locally contextualized SSP1–SSP3 assumptions were operationalized through alternative growth settings and protection of ecosystem-based adaptation opportunity areas, flood-prone land, and tourism areas. From a 2020 urban extent of 208.42 km^2, the mean simulated urban area reached 437.02 km^2 under SSP1, 487.37 km^2 under SSP2, and 564.81 km^2 under SSP3. High probability growth clusters were concentrated in coastal lowlands, peri-urban and industrial development zones, and western development corridors. Agricultural land accounted for the largest share of projected conversion, with combined cropland and rice losses increasing across the scenarios. Landscape analysis indicated increasing urban coalescence in the main simulations; however, a constant area sensitivity showed that part of this pattern resulted from differences in total urban growth quantity. Additional sensitivity experiments confirmed that scenario divergence reflected the combined influence of growth settings and spatial protection. The framework provides a transparent approach for linking locally contextualized SSP narratives with empirical growth patterns, spatial planning constraints, uncertainty, and comparative urban futures analysis.

1. Introduction

Rapid urbanization is reshaping landscapes and transforming ecosystems worldwide, with profound implications for sustainability, environmental management, and climate risk (Garschagen & Romero-Lankao, 2015; Güneralp & Seto, 2013; IPCC, 2023; Muneer, 2023). By 2050, about 68% of the world's population is projected to reside in urban areas (UNDESA, 2018), of which most of this growth is expected to be predominantly in developing regions of Asia and Africa (UN-Habitat, 2022). Generally, urbanization is considered a driver of economic growth and infrastructural development (Liu et al., 2024); however, it can also intensify pressures on land, ecosystems, and natural resources, thereby resulting in habitat loss, agricultural decline, and increased exposure to environmental hazards (Cheng et al., 2023; Garschagen & Romero-Lankao, 2015; Huong & Pathirana, 2013). In coastal and low-lying regions, urban expansion amplifies flood risk and exacerbates vulnerability to sea-level rise and extreme weather events (Hallegatte et al., 2013; IPCC, 2023; Magnan et al., 2022). Managing this

* Corresponding author at: Development of Urban and Rural Regions, Institute of Geodesy and Geoinformation (IGG), University of Bonn, Nußallee 1, Bonn 53115, Germany.
E-mail address: oobaitor@uni-bonn.de (O.S. Badmos).

https://doi.org/10.1016/j.landusepol.2026.108431
Received 1 November 2025; Received in revised form 30 October 2026; Accepted 16 November 2026
Available online 24 November 2026
0264-8377/© 2026 The Authors. Published by Elsevier Ltd. This is an open access article under the CC BY license (http://creativecommons.org/licenses/by/4.0/).
Open access funding enabled and organized by Projekt DEAL.

expansion in a sustainable manner has therefore become a central challenge for urban planners and policymakers, especially in low-lying coastal regions where much of future population growth is expected to occur (Reimann et al., 2023).

To manage these challenges, there has been a major emphasis on integrating ecosystem-based, adaptation-oriented, and land governance measures within urban development strategies (Mills et al., 2020; Wamsler, 2015). Ecosystem-Based Adaptation (EbA), for instance, promotes the use of biodiversity and ecosystem services to help people adapt to the adverse effects of climate change while also improving food security and providing additional livelihood opportunities (Bhusal et al., 2022; CBD, 2009; Mercado et al., 2023). In the same vein, land governance, which refers to the rules, processes, and structures that govern land access, use, and management for competing interests (Palmer et al., 2009), can play a critical role in urban planning. Within this context, land governance will entail a balanced urban planning that can align social, economic, and ecological concerns (Udessa, 2024). However, despite their growing recognition, EbA and related spatial land-governance priorities remain less systematically integrated into quantitative urban growth models. This limits understanding of how alternative development and protection strategies may shape the long-term spatial structure of cities.

The Shared Socioeconomic Pathways (SSPs) provide coherent global narratives that describe plausible futures of societal and environmental development (O'Neill et al., 2014). Each pathway captures divergent scenarios of economic growth, governance capacity, and environmental stewardship (O'Neill et al., 2014). For instance, SSP1 ("Sustainability") envisions strong governance and proactive environmental policy; SSP2 ("Middle of the Road") reflects moderate, uneven progress; SSP3 ("Regional Rivalry") depicts fragmented institutions and weak land-use regulation; SSP4 ("Inequality") highlights unequal access to resources and uneven governance capacity; and SSP5 ("Fossil-fueled Development") describes rapid, market-driven growth coupled with high energy demand and limited environmental concern (O'Neill et al., 2017). Although widely applied at global and national scales and increasingly within urban and regional studies (Chen et al., 2019; He et al., 2023; Hou et al., 2023; Huang et al., 2022; van Vuuren et al., 2014), their downscaling and operationalization for city-scale spatial planning remain comparatively limited. This is particularly important where local development pathways must be interpreted alongside land-management and adaptation priorities.

Urban growth models (UGMs), particularly Cellular Automata (CA)-based approaches, provide established tools for examining the spatial consequences of alternative socioeconomic and land-management scenarios (Clarke et al., 1997; Liu et al., 2019; Wang, Guo, et al., 2021; Wu et al., 2010). Their integration with machine-learning methods, including Random Forest and support vector machines, can further improve the empirical representation of spatial development potential (Badmos et al., 2019; Rienow & Goetzke, 2015; Wang, Liu, et al., 2021). SSPs have already been integrated with spatially explicit urban and land-use models across global, regional, metropolitan, and city scales (Bachofer et al., 2026; Chen et al., 2020; Siabi et al., 2025; Wu et al., 2025; Xiao et al., 2025). These studies demonstrate the growing maturity of SSP-based spatial modelling. The remaining methodological challenge is therefore not the coupling of SSPs with urban growth models itself, but the development of transparent and locally grounded procedures for translating qualitative SSP narratives into both development dynamics and spatial land-management constraints, particularly where adaptation, ecosystem conservation, hazard exposure, and competing land-use priorities must be represented simultaneously.

Against this background, this study develops and evaluates a hybrid framework for translating locally downscaled SSP narratives into spatially explicit urban growth scenarios using a Random Forest–Cellular Automata structure in one of the most important adaptation frontiers: coastal cities (Wannewitz et al., 2024). Hue, Central Vietnam, provides a relevant case because it combines substantial urban development pressure with high exposure to climate related hazards and strong competing demands for environmental conservation, tourism, infrastructure, and land development (Tuan, 2022; World Bank, 2020). The city has undergone considerable expansion associated with demographic and economic change (Tuan, 2022; World Bank, 2020), while its coastal and low-lying setting contributes to exposure to flooding, sea-level rise, and other climate related hazards (Phuong et al., 2023; Sett et al., 2024). At the same time, Hue's development strategy emphasizes its role as a regional center for culture, tourism, education, and marine based economic activities (TTH, 2023), creating potentially competing demands for urban land and environmental protection. Within this context, the study addresses four questions: (i) How do locally parameterized SSP1–SSP3 scenarios differ in the magnitude and spatial distribution of simulated urban growth in Hue by 2050? (ii) Where do consistently simulated clusters and broader directions of new urban development emerge under each scenario? (iii) To what extent does the simulated urban expansion encroach on existing land-use categories under the alternative pathways? and (iv) How does the spatial configuration of the resulting urban landscape differ among the scenarios, and to what extent do these differences persist when variation in total urban growth quantity is controlled?

The contribution of the study lies in the operationalization workflow. The framework links participatory SSP downscaling with empirically derived urban growth propensity from Random Forest, scenario specific spatial protection of EbA opportunity areas, flood-prone land, and tourism areas, and stochastic urban growth simulations of alternative 2050 urban patterns. In this way, qualitative scenario narratives are translated into an explicit sequence of assumptions concerning development pressure and spatial protection that can be traced through to their simulated spatial consequences. The analysis further incorporates ensemble uncertainty and controlled sensitivity experiments to distinguish the effects of scenario specific growth settings from those of spatial protection and urban growth quantity. The resulting simulations are therefore interpreted as conditional representations of plausible urban futures under specified scenario assumptions. This provides a transferable framework for examining how locally contextualized socioeconomic pathways and competing land management priorities can be represented within spatially explicit urban scenario modelling.

2. Study area and data

This study was conducted in the city of Hue, located in central Vietnam (Fig. 1). Before January 1, 2025, the city was referred to as Thua Thien Hue province, but now it is a centrally governed municipality, presently known as Hue City (TTH, 2023). The study encompasses a natural land area of 4947.11 km^2. It is geographically located between 16° and 16.8° North latitude and 107° and 108.2° East longitude. It is bordered by the South China Sea to the east and shares its western boundary with Laos. Hue has a tropical monsoon climate with an average annual rainfall exceeding 3000 mm, mostly concentrated from September to December. Its ecosystem mosaic includes wetlands, mangrove belts, forests, and coastal dunes, many of which can provide natural buffers against flooding and erosion (Nehren et al., 2017). The total population of the city is 1160,224, comprising 612,827 residents in urban areas and 547,397 in rural regions (Hue Statistics Office, 2022). Historically recognized as the imperial capital of Vietnam, Hue carries deep cultural heritage, reflected in its architecture, traditions, and its importance as a center of learning and spirituality. Hue, like other regions in Vietnam, has a high vulnerability to natural hazards, making it one of the most disaster-prone regions in the country (Chaudhry & Ruysschaert, 2008; Vu, Obaitor, Grobusch, et al., 2025).

The study utilized both geospatial data sets and qualitative data to simulate future urban growth (2050) under different SSPs. We chose 2050 as the year for simulation because the latest master plan for Hue also included the vision for 2050 for the city (TTH, 2023), which was also included in the scenario development. We also defined urban in this

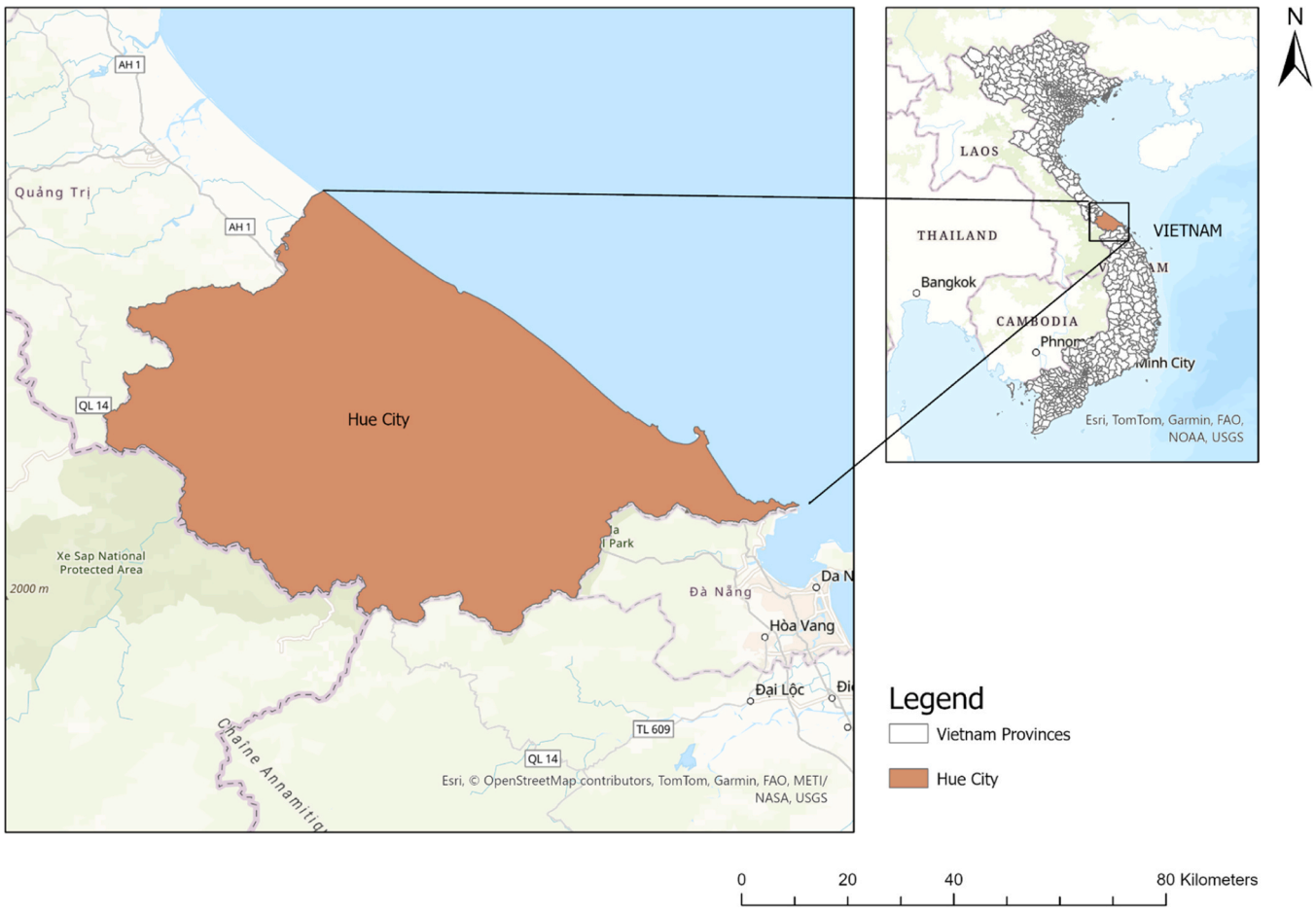

Fig. 1. The study area of Hue City.

study as "urban land cover and land use, impervious surfaces, and other manifestations of the built environment" (Seto et al. 2011 p. 2).

The geospatial dataset included historical land-use maps for 2000, 2010, and 2020 from the JAXA/EORC Annual Land Use and Land Cover Maps of Mainland Vietnam, Version 21.09, Level 2 (JAXA, 2021; Phan et al., 2021), together with a TanDEM-X-based digital elevation model obtained from the German Aerospace Center (DLR) (González et al., 2020). Additional spatial datasets included road networks, places of worship, social areas, industrial and mining areas, railways, flood-prone areas, prospective EbA areas, and tourism locations obtained from OpenStreetMap and provincial government agencies in Hue, including the Department of Transport and the Department of Natural Resources and Environment. All spatial datasets were transformed to WGS 84/UTM Zone 48 N (EPSG:32648) and harmonized to a 30-m grid. Data preprocessing and analysis were undertaken using Python and ArcGIS Pro 3.2.

We obtained the qualitative data through World Café discussions and key informant interviews (KII) with experts in Hue. The goal of the World Café discussions was to downscale the global SSPs to the Hue city level. Through KII, we quantified the narratives in the downscaled SSP, verified scenario plausibility, and assessed the modeled results. In this part of the study, pseudonyms were used during the data collection, data analysis, and data storage for all the participating individuals, adhering strictly to ethical protocols concerning confidentiality and informed consent.

3. Methodology

This study applies a hybrid, locally contextualized urban growth modelling framework that translates downscaled SSP narratives into spatially explicit 2050 urban scenarios. The workflow comprises six linked steps (Fig. 2): (i) participatory downscaling of SSP1–SSP3 into locally relevant growth and spatial protection assumptions; (ii) estimation of urban growth propensity using Random Forest (RF) and historical calibration and temporal validation of the urban growth CA model; (iii) coupling of the RF-derived propensity surface with SSP specific spatial constraints for EbA, flood-prone, and tourism areas; (iv) stochastic simulation of SSP1–SSP3 futures using 100 Monte Carlo (MC) realizations, supported by controlled sensitivity analyses; (v) qualitative plausibility assessment of the simulated future patterns using field observations and expert review; and (vi) analysis of projected urban growth magnitude, spatial hotspots, land-use encroachment, and landscape configuration.

3.1. Downscaling global SSPs to Hue's city-level quantitative and spatial parameters

SSP operationalization combines qualitative storylines describing alternative development trajectories with quantitative assumptions that enable these narratives to be represented in modelling applications (O'Neill et al., 2014, 2017).

3.1.1. Developing the storyline narratives

The global SSPs (O'Neill et al., 2017) were downscaled to reflect the specific socioeconomic, environmental, and governance context of Hue. The downscaling process translated global assumptions related to demographics, human development, economic growth, policy orientation, technology, and environmental management into locally relevant

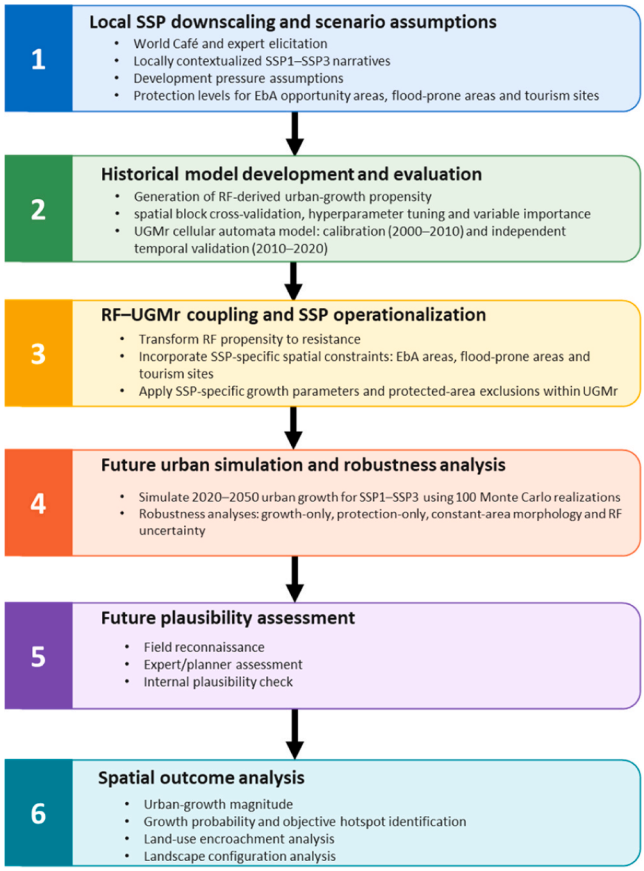

Fig. 2. Integrated SSP–RF–Urban Growth Modelling Framework.

narratives and parameters. This ensured that the resulting scenarios were both consistent with global trajectories and tailored to Hue's unique development trajectories. Three global SSPs were selected as the most relevant to Hue's context: SSP1, SSP2, and SSP3 (Vu, Obaitor, Katzschner, et al., 2025). An initial set of localized scenario drafts was developed through a comprehensive literature review and then refined through a participatory World Café process (see S2). Stakeholders, including government officials, NGOs, civil society representatives, and academics, were invited to review and adjust the scenario narratives in two iterative sessions held in July 2022 and March 2023. The first session focused on revising and contextualizing the draft narratives, while the second validated the combined versions, resulting in the final downscaled SSP storylines for Hue. All discussions were conducted in Vietnamese to facilitate open and inclusive participation.

3.1.2. *Quantification of storylines from the downscaled SSPs*

We conducted a thematic analysis of the downscaled SSP storylines to identify the dominant themes relevant to Hue's future urban development context. Three recurring priorities emerged across the scenarios: conservation of land uses with EbA potential, protection of flood-prone areas, and preservation of tourism areas. Their relative emphasis varied among SSP1–SSP3 in accordance with the underlying assumptions concerning planning priorities, institutional capacity, and policy implementation. The scenarios also differed in their assumed intensity of future urban expansion.

Four key informant interviews (KIIs) were conducted with domain experts in tourism, EbA and forest management, urban development, and flood management. For each SSP, experts were asked to assess the proportion of relevant land use areas that should remain protected from future urban development and to characterize the expected intensity of urban expansion relative to current trends in Hue. Participants were purposively selected from academia and relevant government institutions based on their sector specific expertise. The elicitation was domain specific, so the estimates were not pooled or statistically averaged across experts. Values provided by the relevant expert for each thematic domain were adopted directly as the corresponding scenario assumptions. Individual estimates, qualitative justifications, and the final values used in the model are reported in Table S1.

3.1.3. *Spatial translation*

The quantified SSP assumptions were translated into scenario specific CA-based urban growth parameters (diffusion, breed, spread, slope resistance, and road gravity) and spatial exclusion layers representing protection of EbA opportunity areas, tourism areas, and flood-prone land. This process operationalized qualitative SSP narratives into quantitative, spatially explicit model inputs for the 2050 simulations (explained in detail in 3.3).

3.2. *Hybrid Random Forest–Cellular Automata Modeling*

This step involves the coupling of the RF classifier with the UG model to simulate spatially explicit urban growth in Hue. The RF estimates empirical spatial propensity for urban growth, while the CA model simulates the spatial processes through which growth is allocated across the landscape.

3.2.1. *Random Forest urban growth propensity model*

The RF classifier (Breiman, 2001) was trained on observed urban transitions between 2010 and 2020. Cells that were non-urban in 2010 and urban by 2020 were coded as conversion events (1), while cells remaining non-urban were coded as non-conversion (0). Cells already urban in 2010 were excluded from model training. The analysis included 5471,132 eligible cells, of which 143,009 converted between 2010 and 2020, representing a landscape conversion prevalence of 2.61%.

Sixteen spatial predictors represented accessibility, existing urban structure, topography, land use, and proximity to infrastructure and economic activities. This included proximity to existing urban land, cropland, roads, railways, the Hue expressway, water, commercial and social areas, industrial and mining locations, local urban proportion, elevation, and slope. Predictor selection was informed by previous urban growth studies (Carlino & Saiz, 2019; D'Amour et al., 2017; Güneralp & Seto, 2013; Obaitor et al., 2025; Trung Thanh et al., 2021; Verma & Das, 2024). The complete variable definitions are provided in Table S3.

All 143,009 conversion cells were retained, while an equal number of stable non-urban cells were sampled without replacement to address class imbalance, producing a balanced training dataset of 286,018 observations. A fixed random seed was used for reproducibility. The resulting case control design changes the observed landscape prevalence of conversion, so RF outputs were interpreted as relative urban growth propensity.

Spatial dependence was addressed using five-fold spatial block cross-validation with approximately 5 km blocks, balancing spatial separation with sufficient conversion observations and spatial coverage within each fold. Hyperparameters were selected from 15 randomized combinations evaluated across the five folds (75 fits), using ROC-AUC as the optimization criterion. The final model used 200 trees, entropy splitting, maximum depth 40, sqrt feature sampling, minimum leaf size 5, minimum split size 10, and bootstrap sampling. Spatial validation was consistently high across folds (ROC-AUC 0.956–0.963; balanced accuracy 0.892–0.909). Pooled out-of-fold performance yielded ROC-AUC = 0.960, balanced accuracy = 0.900, sensitivity = 0.894, and specificity = 0.906. Fold-specific results are reported in Table S4.

Permutation importance calculated on held-out spatial folds identified proximity to existing urban land as the strongest predictor, followed by proximity to cropland, road accessibility, elevation, and local urban proportion (Table S5). Following validation, the RF was refitted to the complete balanced 2010–2020 sample and applied to corresponding

2020 predictor surfaces to generate the propensity layer used for future simulations.

Prediction uncertainty was assessed using a five-member spatial-fold ensemble. Mean cell-wise standard deviation was 0.024 (median = 0.017; 95th percentile = 0.073), while the ensemble-mean propensity surface was strongly correlated with the full-data RF prediction (r = 0.995; MAE = 0.013; RMSE = 0.020), indicating high spatial stability (Table S6).

The propensity was inverted before coupling with the CA-based model such that locations with higher empirical urban growth propensity received lower resistance, whereas locations with lower propensity received higher resistance.

3.2.2. Cellular Automata Simulation

Urban growth was simulated using the urban growth model reduced (UGMr) (Goetzke, 2011; Jantz et al., 2010; Schmitz et al., 2007), derived from the original SLEUTH cellular automata framework (Clarke, 2008; Clarke et al., 1997). The UGMr was originally introduced within the XULU modelling framework to allow calibration using two temporally separated urban maps and multiple-resolution validation (Goetzke, 2011; Rienow & Goetzke, 2015). The UGMr represents urban expansion through four growth processes: spontaneous growth, new spreading center growth, edge growth, and road-influenced growth. These processes are controlled by five coefficients: dispersion, breed, spread, road gravity, and slope resistance (Jantz et al., 2010). For the present study, the UGMr growth logic was implemented in Python for faster processing and reproducibility.

Four spatial inputs were required by the UGMr component: a binary urban map, slope, a weighted transport layer, and an exclusion/resistance layer. The transport layer ranged from 1 to 27, with 1 representing cells without road influence and values above 1 representing increasing road influence. During each annual simulation step, candidate urban cells generated through the four growth processes were evaluated according to slope, the critical-slope threshold, road influence, and cell-specific resistance. Resistance ranged from 0, indicating no restriction, to 1, indicating complete exclusion from conversion.

3.2.3. UGMr calibration, independent temporal validation, and retrospective hybrid reconstruction

UGMr was calibrated against observed urban change from 2000 to 2010, using the 2000 urban map as the initial condition and the 2010 map as the calibration target. Water was the only hard exclusion during calibration, and the critical slope was fixed at 23. The five growth coefficients were evaluated through a sequential coarse-to-fine search. An initial search using values of 1, 50, and 100 identified the region of strongest model performance. Road gravity showed little sensitivity across otherwise similar parameter combinations, and it was fixed at 70 during the subsequent fine search. The refined calibration evaluated dispersion at 1, 5, 10, and 20; breed at 1, 10, 20, 30, and 50; spread and slope resistance at 70, 80, 90, 95, and 100, yielding 500 parameter combinations. The strongest candidate sets were subsequently assessed using 100 MC realizations. The retained coefficients were dispersion = 1, breed = 10, spread = 80, road gravity = 70, and slope resistance = 70 (Table S7). These values were frozen before temporal validation and were not adjusted using the 2020 observations.

Model evaluation emphasized agreement in newly urbanized cells, as persistence can inflate whole-map agreement. At each spatial scale s, observed and simulated new growth cells were aggregated into spatial windows, and agreement was calculated as:

$$A_s = \frac{\sum_j \min(O_{j,s}, S_{j,s})}{\sum_j \max(O_{j,s}, S_{j,s})}$$

where $O_{j,s}$ and $S_{j,s}$ are the observed and simulated new urban cell counts within window j. At the native 30 m resolution, this is equivalent to the Figure of Merit (FoM):

$$\mathrm{FoM} = \frac{H}{H + M + F}$$

where H denotes hits, M misses, and F false alarms. Agreement was evaluated at 30, 60, 120, 240, 480, 960, and 1920 m. Finer scales received greater weight using

$$w_s = \exp[-0.1(s-1)]$$

and the overall change-focused score was calculated as:

$$\mathrm{MRV}_{\mathrm{change}} = \frac{\sum_s w_s A_s}{\sum_s w_s}$$

Growth quantity was evaluated independently as:

$$Q = \frac{\min(G_{\mathrm{obs}}, G_{\mathrm{sim}})}{\max(G_{\mathrm{obs}}, G_{\mathrm{sim}})}$$

where G_{obs} and G_{sim} are observed and simulated new growth cell counts. Candidate parameter sets were selected jointly using change focused MRV, FoM, and quantity fit. A conventional full map of multiple resolution score and persistence benchmark were retained only as diagnostics because unchanged cells can inflate apparent agreement.

Independent temporal validation was conducted for 2010–2020 using the observed 2010 urban map as the initial condition and the 2020 map as the validation target. The calibrated coefficients, water-only exclusion, slope and transport inputs, spatial scales, and weighting scheme were retained unchanged. One hundred MC realizations were performed, with ensemble means and 95% confidence intervals calculated for change-focused MRV, FoM, quantity fit, and simulated urban extent.

The RF-derived resistance described in Section 3.2.1 was introduced only after this independent validation. A separate 2010–2020 retrospective reconstruction used the frozen UGMr coefficients but replaced the water-only exclusion with the RF-plus-water resistance surface (Table S8). This improved change-focused MRV from 0.252 to 0.272, FoM from 0.208 to 0.223, and quantity fit from 0.778 to 0.923, while reducing mean urban extent overprediction from 39.78 km^2 to 13.75 km^2. This was specifically done to examine whether the RF-derived spatial resistance improved the spatial allocation and quantity of simulated growth relative to the independently validated water-only UGMr configuration. No model coefficients were recalibrated on the basis of this retrospective reconstruction. The corresponding 2020 RF-plus-water surface then formed the baseline for the 2020–2050 SSP simulations. The experimental design and numerical performance of the historical calibration, independent temporal validation, and retrospective RF–UGMr reconstruction are summarized in Supplementary Tables S8 and S9, respectively.

3.3. Spatially explicit operationalization of the SSPs within the UGMr model

The locally downscaled SSP narratives were operationalized in UGMr through two complementary components: scenario-specific urban growth settings and scenario specific spatial protection. Within SLEUTH models, alternative development pathways can be represented by modifying growth coefficients, spatial exclusions, or both (Badmos et al., 2019; Jantz et al., 2010; Mubea, K. and Menz, G, 2014). In this study, both components were varied to represent the locally derived differences among SSP1–SSP3. The resulting simulations are therefore interpreted as conditional outcomes of the specified scenario assumptions of Hue's future development.

3.3.1. Scenario definition and parameterization

The three configurations represent contrasting combinations of development pressure and land protection. SSP1 reflects stronger planning coordination and greater implementation of environmental protection; SSP2 represents continuation of intermediate development and protection conditions; and SSP3 represents comparatively greater development pressure combined with weaker implementation of spatial restrictions. These configurations were treated as internally consistent modelling assumptions, rather than as causal estimates of the effects of governance or economic growth.

The calibrated UGMr parameterization was retained as the reference configuration for SSP2, representing a continuation of current development conditions. The scenario specific growth settings for SSP1 and SSP3 were informed by the locally downscaled SSP narratives and subsequent qualitative expert interviews. The downscaling process identified contrasting patterns of urban development including coordinated spatial expansion under SSP1, continuation of existing urban and suburban development trends under SSP2, and less controlled, increasingly fragmented expansion under SSP3. The qualitative interviews further provided insights into urban expansion, the emergence of new spreading centers, and differences in development pressure across the scenarios. These inputs informed the selection and directional adjustment of the UGMr coefficients governing spontaneous growth, formation of new spreading centers, and edge expansion.

To operationalize these differences, selected UGMr parameters were adjusted relative to the calibrated SSP2 configuration. Under SSP1, the breed was reduced from 10 to 5, spread from 80 to 70, and the critical-slope threshold from 23 to 20, while dispersion remained at 1. These settings represented more controlled development, reduced formation of new spreading centers, slower edge expansion, and greater restriction of development on steeper terrain. Under SSP3, dispersion was increased from 1 to 5, breed from 10 to 20, spread from 80 to 90, and the critical-slope threshold from 23 to 30, representing greater potential for dispersed expansion, new development centers, edge growth, and conversion on less suitable terrain. Road gravity and slope resistance were retained at their calibrated values of 70 across all scenarios. The resulting configurations operationalized the contrasting spatial development trajectories within the UGMr framework, and their combined influence was examined through the controlled sensitivity experiments described in Section 3.3.3. The adopted parameter values are presented in Table 1. Expert-derived protection percentages were interpreted as the proportion of each mapped domain protected from future urban development. Thus, differences among SSPs affected the spatial extent of complete protection.

Table 1
Scenario configuration for urban growth simulation in Hue to 2050.

	Description of scenarios	Spatial Protection	Urban growth parameters
Scenario 1 (SSP1)	Stronger governance, proactive environmental management, coordinated spatial planning, and comparatively strict control of urban expansion.	RF-derived spatial resistance + water hard exclusion; Tourism Opp: 80% EbA opp.: 80% Flood Areas: 60%	Dispersion-1 Breed-5 Spread-70 Road-70 Slope-70 Critical slope −20
Scenario 2 (SSP2)	Urban growth characterized by moderate governance capacity, incremental policy implementation, and continued reliance on existing planning practice	RF-derived spatial resistance + water hard exclusion; Tourism Opp: 50% EbA opp.: 60% Flood Areas: 40%	Dispersion-1 Breed-10 Spread-80 Road-70 Slope-70 Critical slope −23
Scenario 3 (SSP3)	Urban growth characterized by weak governance and minimal enforcement of environmental controls, with economic and urban pressures driving land conversion	RF-derived spatial resistance + water hard exclusion; Tourism Opp: 30% EbA opp.: 40% Flood Areas: 15%	Dispersion-5 Breed-20 Spread-90 Road-70 Slope-70 Critical slope −30

*Opp= Opportunities

3.3.2. Development of scenario-specific exclusion layers

Spatial constraints were derived from the Hue Provincial Master Plan (TTH, 2023) and associated provincial geospatial datasets and were grouped into three principal categories identified as relevant to the localized SSPs: (i) EbA opportunity areas, represented by mapped biodiversity corridors, ecological landscapes, and wetlands; (ii) flood-prone areas, represented by the mapped extent of areas affected by the severe 2022 flooding in Hue; and (iii) tourism development zones: areas prioritized for cultural and ecotourism functions where urban growth is limited to preserve landscape and heritage values. The severity of the October 2022 flood event is independently documented by Hoang Nam et al. (2024), who reported extensive inundation across the city. The flood layer was used as a locally grounded spatial planning constraint rather than as a probabilistic projection of future flood hazard.

The 2020 RF-plus-water resistance surface described in Section 3.2 provided the baseline spatial resistance for future simulations. Water remained completely excluded from development, while all other baseline resistance values were retained unless a cell was selected for additional SSP-specific protection. Because the expert elicitation specified how much of each domain should be protected but did not identify the exact locations to prioritize, a reproducible spatially neutral allocation procedure was applied. For the vector layers (i.e., EbA, flood-prone, and tourism areas), eligible 30 m cells were assigned a fixed random ordering using a predefined seed. Scenario specific protected subsets were then selected according to the required proportions using the same ordering across SSPs. This produced nested protection sets, such that the SSP3 protected subset was contained within SSP2 and the SSP2 subset within SSP1. The approach ensured that differences among scenarios represented progressively changing protection extent rather than unrelated spatial realizations.

For each SSP, the selected EbA, flood, and tourism subsets were combined using a logical union. Any cell selected for protection in at least one domain was assigned complete exclusion from future urban development, while all remaining cells retained their RF-derived baseline resistance:

$$R_{i,s} = \begin{cases} 1, & \text{if} i \in \mathscr{P}_s, \\ R_{\mathrm{RF},i}, & \text{otherwise}, \end{cases}$$

where $R_{i,s}$ is the final resistance of cell i under scenario s, $R_{RF,i}$ is its baseline RF-derived resistance, and P_s is the union of locations protected under the corresponding SSP. This formulation allowed the scenarios to modify the extent of complete spatial protection while preserving the empirically estimated pattern of urban growth resistance elsewhere.

3.3.3. Scenario Implementation and Sensitivity Analysis

Each SSP was simulated from 2020 to 2050 over 30 annual time steps using 100 MC realizations. The same random-seed sequence was applied across SSP1–SSP3 to enable paired comparison under equivalent stochastic conditions. Two controlled sensitivity experiments were conducted to distinguish the contributions of growth settings and spatial protection to differences among the SSP simulations. In the protection-only experiment, the calibrated UGMr configuration was held constant while the SSP-specific protection layers were varied. In the growth setting experiment, the SSP-specific UGMr configurations were varied, while all scenarios used the same 2020 RF-plus-water resistance surface.

Both experiments used 100 MC realizations and the same random-seed sequence as the main simulations. The effects of spatial protection and growth settings were calculated as differences in mean

simulated 2050 urban extent relative to the common reference configuration. Their interaction was calculated as the difference between the combined scenario effect and the sum of the corresponding protection-only and growth-setting effects. These comparisons were used to assess the relative contributions of the two scenario components and their interaction to simulated urban expansion.

3.4. Plausibility assessment of future urban growth

Historical model performance was evaluated quantitatively for 2000–2020 as described in Section 3.2.3. Future simulations were assessed qualitatively for plausibility, since observed data are not available for validating the 2050 outcomes. Field reconnaissance was undertaken at selected locations identified by the simulations as potential areas of future development, providing contextual information on existing land use, infrastructure development, development pressure, and physical constraints.

The SSP1–SSP3 simulation maps were subsequently reviewed by local experts. Participants assessed whether the simulated spatial patterns were consistent with plausible development trajectories under the assumptions of each SSP, focusing on the direction of expansion, emerging development corridors, and locations likely to experience stronger or weaker development pressure. Their observations were synthesized narratively to identify recurring areas of agreement, concern, and scenario-specific interpretation.

The participating experts had also contributed to the earlier SSP parameterization. The assessment was therefore treated as an internal plausibility and consistency check, not as independent validation or evidence of predictive accuracy. Expert feedback was used primarily to complement the contextual interpretation of the simulated spatial patterns.

3.5. Analysis of Simulated Urban Growth Outcomes

3.5.1. Growth hotspots and land-use conversion

Spatial concentrations of consistently simulated growth were identified from the ensemble probability surfaces. High-probability growth clusters were defined as 8-neighbour contiguous areas with a probability of new urbanization of at least 0.75 and a minimum area of 1 km^2. Potential land-use conversion was assessed by overlaying simulated new urban cells for 2020–2050 with the 2020 JAXA Level-2 land-use map. The categorical raster was aligned to the 30-m UGMr grid in EPSG:32648 using nearest-neighbor resampling. For each of the 100 MC realizations, new urban cells were assigned their corresponding 2020 land-use class, and class-specific converted areas were summarized as ensemble means and 95% confidence intervals.

3.5.2. Urban landscape configuration analysis

Urban landscape configuration was evaluated for the observed 2020 urban pattern and the simulated 2050 landscapes under SSP1–SSP3. Landscape metrics are widely used to quantify changes in urban form, spatial fragmentation, and development structure (Herold et al., 2005; Jantz et al., 2010; Seto et al., 2012). Three complementary class-level metrics were selected: Mean Patch Size (MPS), Patch Density (PD), and Landscape Shape Index (LSI), following established landscape-pattern analysis approaches (Herold et al., 2005; McGarigal & Marks, 1995). MPS describes the average size of discrete urban patches and therefore indicates the degree of urban aggregation; PD measures the frequency of urban patches across a fixed landscape area and provides an indicator of spatial dispersion; and LSI characterizes the complexity of the urban/non-urban boundary. These metrics allow comparison of the spatial organization of urban development across the alternative SSP configurations without attributing observed differences to any single scenario assumption.

Metrics were calculated for each of the 100 MC realizations using the complete simulated 2050 urban extent, comprising existing 2020 urban land and new development between 2020 and 2050. Urban patches were delineated using eight-neighbour connectivity, whereby cells sharing an edge or corner were treated as part of the same patch (Herold et al., 2005). The number of patches (N_p) was also recorded as a supporting measure of landscape configuration.

MPS was calculated as

$$MPS = \frac{A_{u,\mathrm{ha}}}{N_p}$$

where $A_{u,ha}$ is the total urban area in hectares. Patch density was calculated relative to the fixed valid analysis landscape rather than urban area:

$$PD = \frac{N_p}{A_{L,\mathrm{ha}}} \times 100$$

where $A_{L,ha}$ is the total fixed valid landscape area in hectares, yielding patches per 100 ha. Use of a constant landscape denominator permits direct comparison among the baseline and future scenarios. LSI was calculated as:

$$\mathrm{LSI} = \frac{0.25E}{\sqrt{A_{u,m^2}}}$$

where E is the exposed urban/non-urban boundary length in meters and A_{u,m^2} is the urban area in m^2. Boundary length was derived from exposed four-neighbour cell edges, consistent with raster-based landscape-shape measurement (McGarigal & Marks, 1995).

For both land-use conversion and landscape metrics, ensemble means, 95% confidence intervals for the means, and 5th–95th percentile ranges were calculated across the 100 MC realizations for each SSP. The 95% confidence intervals were estimated as the mean ± 1.96 times the standard error (SD/$\sqrt{\mathrm{n}}$), where SD is the sample standard deviation and n = 100. The 5th and 95th percentiles were calculated from the distribution of values across the individual realizations, representing the central 90% of simulated outcomes. For land-use categories comprising multiple JAXA classes, conversion areas were first aggregated within each realization before calculating the ensemble statistics. These measures characterize stochastic variation under the specified scenario configurations

Identical random-seed sequences across SSPs also enabled paired scenario comparisons, reducing the influence of stochastic variation on between-scenario differences. A constant-area sensitivity analysis examined whether differences in urban configuration persisted when growth quantity was held equal across SSPs. The common growth quantity was defined using the smallest mean expansion among the three scenarios. Cells were ranked by ensemble conversion probability, and an equal number of highest-probability cells was retained for each SSP before adding the existing 2020 urban extent. Probability ties at the selection threshold were resolved across 30 random realizations. The resulting metrics were used as a diagnostic of spatial configuration under equivalent growth quantity.

4. Results

4.1. Urban Growth Magnitude under SSP1-SSP3

The three SSP configurations produced clearly differentiated urban expansion trajectories between 2020 and 2050 (Fig. 3). From an observed urban extent of 208.42 km^2 in 2020, the mean urban extent across the 100 MC realizations reached 437.02 km^2 under SSP1, 487.37 km^2 under SSP2, and 564.81 km^2 under SSP3. This represents additional urban growth of 228.60 km^2, 278.95 km^2, and 356.38 km^2, respectively. Relative to the 2020 baseline, urban extent increased by 109.68% under SSP1, 133.84% under SSP2, and 170.99% under SSP3. SSP2 generated approximately 50.35 km^2 more urban land than SSP1,

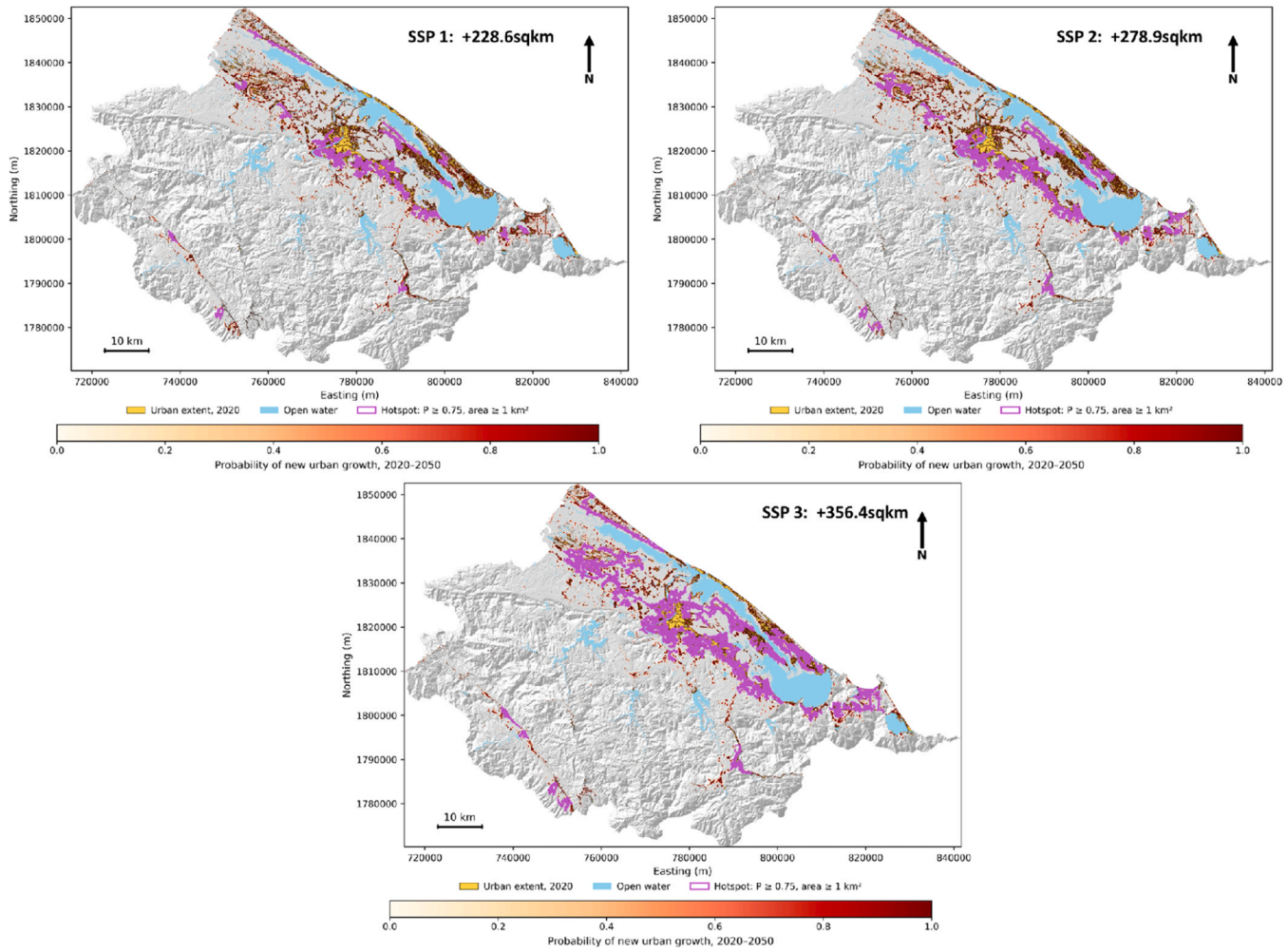

Fig. 3. Future scenarios of urban growth under different shared socioeconomic pathways (SSP1-3) in Hue.

while SSP3 exceeded SSP2 by 77.44 km^2 and SSP1 by 127.79 km^2. The ordering was consistent across the simulations, with SSP1 producing the smallest urban footprint, SSP2 an intermediate extent, and SSP3 the largest extent by 2050.

Variation among MC realizations was small compared with the differences among scenarios. The 95% confidence intervals for projected 2050 urban extent were 436.95–437.10 km^2 for SSP1, 487.28–487.46 km^2 for SSP2, and 564.71–564.91 km^2 for SSP3. The narrow intervals indicate high consistency in simulated urban extent within each scenario and clear separation among the three conditional pathways.

4.2. *Spatial distribution and potential growth hotspots in Hue*

The ensemble simulations show increasing spatial concentration of future urban growth from SSP1 to SSP3 (Fig. 3). Using a new-growth probability threshold of ≥ 0.75 and a minimum contiguous area of 1 km^2, 29 hotspot clusters were identified under SSP1, 30 under SSP2, and 42 under SSP3. Across the scenarios, these clusters were concentrated within recurring broader development zones: the coastal lowlands and flood-prone areas, industrial development corridors, the urban periphery of central Hue, lower plains adjoining mountainous areas, and corridors extending toward the Laos border. These spatial tendencies became more extensive under SSP3.

Projected growth remained prominent in the coastal lowlands, including flood-prone areas, across all three scenarios. Field observations recorded ongoing building and infrastructure development as well as resettlement in communes such as Thuan An, where flooding occurs at least three times a year. Expert assessments linked continued development pressure to land availability, accessibility to central Hue, and the economic importance of the coastal and lagoon zone:

"*Floods occur approximately 1–3 times per year, impacting livelihoods and assets. However, the government accepts this trade-off due to the limited availability of land for urban expansion. When there is a scarcity of land for urban development, areas at risk of flooding are still utilized for expansion. Some of the coastal areas play a crucial role in the economic development of Hue, and also their proximity to the inner city of Hue allows for the utilization of existing infrastructure to support expansion into neighboring regions.*"

(Participant A, June 2024)

"*The marine and lagoon economies are becoming the driving force for the development of Hue, creating a new dynamic for the entire region. This contributes significantly to leveraging the advantages of tourism and fisheries development.*"

(Participant C, June 2024)

Projected growth was also concentrated around existing and planned industrial areas. Field reconnaissance in Phong Hien, where a planned industrial estate is located, showed ongoing building and road development, consistent with the modelled concentration of future expansion along these corridors.

Another recurring growth zone occurred across the lower plains adjoining Hue's mountainous areas, with the spatial extent becoming particularly pronounced under SSP3. Experts associated this direction of development with infrastructure investment, ecotourism, improved urban–rural connectivity, and development around border-linked

settlements:

"*Urban development in mountainous areas has emerged as a strategy to address the urban-rural imbalance in Hue Also, the mountainous areas have potential for ecotourism, prompting government investments in infrastructure, such as roads and electricity, to support tourism and connectivity.*"

(Participant B, June 2024)

"*In the mountainous area, the A Dot border gate, located in A Luoi district, serves as a significant point of development. Consequently, the state has invested in infrastructure development in the surrounding areas. Additionally, some urban areas in Nam Dong district are planned to be developed to establish better connectivity with the border gate area.*"

(Participant C, June 2024)

The simulations further indicated outward expansion beyond the existing central urban area. This pattern was considered plausible by experts in relation to access to existing infrastructure and Hue's planned development of satellite urban areas:

"Proximity to Hue city allows these areas to leverage existing infrastructure, including electricity networks, water supply, transportation, communication, education, and healthcare services. Also, Hue has a strategic plan to develop satellite urban areas around the city to alleviate pressure on the central urban area."

(Participant A, June 2024)

"Hue's policy is to avoid urban development in the core area to preserve the conservation zone. Consequently, Hue plans to develop satellite urban areas surrounding the core area."

(Participant B, June 2024)

The implication of this policy is that future urban growth may lead to urban sprawl in the municipality. Presently, communes such as Binh Tien and Huong Tho are experiencing increasing urban growth, which may be due to their proximity to Hue City. The simulations also identified growth toward the Laos border, particularly under the higher-growth SSP3 configuration, indicating another potential direction of longer-term urban expansion. This could signify an increase in cross-border activities or a shift toward utilizing previously underdeveloped regions.

4.3. Encroachment on existing land-use and land-cover classes

Projected urban expansion affected the same broad land-use classes across SSP1–SSP3, with the magnitude of conversion increasing progressively from SSP1 to SSP3 (Table 2). Other cropland accounted for the largest absolute area of conversion under all three scenarios. Mean encroachment increased from 108.68 km^2 under SSP1–125.49 km^2 under SSP2 and 148.33 km^2 under SSP3, corresponding to approximately 22.1%, 25.6%, and 30.2% of the 2020 area of this land-use group, respectively. Rice paddies were the second major agricultural land type affected, with projected conversion increasing from 37.70 km^2 under SSP1–50.86 km^2 under SSP2 and 73.95 km^2 under SSP3. This represents approximately 10.4%, 14.0%, and 20.3% of the baseline rice-paddy area. Combined, these results show that agricultural land formed the principal land-use category exposed to simulated urban expansion.

Urban expansion also increasingly affected barren and shrub land. Barren-land conversion increased from 26.05 km^2 under SSP1–32.66 km^2 under SSP2 and 42.61 km^2 under SSP3, equivalent to approximately 25.1%, 31.5%, and 41.1% of its 2020 extent. Shrub showed the highest proportional conversion among the major land-cover classes, with approximately 41.7% of its baseline area converted under SSP1, 46.6% under SSP2, and 53.2% under SSP3, although its absolute converted area remained lower at 19.30, 21.61, and 24.62 km^2, respectively.

Conversion of plantation trees also increased progressively across the scenarios, from 19.74 km^2 under SSP1–25.70 km^2 under SSP2 and 35.01 km^2 under SSP3. In contrast, natural forests experienced comparatively limited proportional encroachment. Mean conversion was 10.04 km^2 under SSP1, 13.06 km^2 under SSP2, and 18.01 km^2 under SSP3, representing approximately 0.39%, 0.51%, and 0.71% of the 2020 natural-forest area. Aquaculture conversion increased from 4.80 km^2 to 7.00 km^2 and 10.89 km^2 across SSP1–SSP3. Open water was unaffected in all scenarios, consistent with its treatment as a hard exclusion in the modelling framework. Although mangrove showed relatively high proportional change, particularly under SSP3, the absolute area involved was minimal because mangrove occupied only 0.24 km^2 within the analysis extent. The land-use results therefore indicate a consistent scenario gradient in which greater simulated urban expansion was accompanied by increasing conversion of agricultural, sparsely vegetated, and selected production landscapes. The corresponding 95% confidence intervals for the ensemble means and 5th–95th percentile ranges of simulated land-use conversion are reported in Table S10.

Table 2
Projected encroachment of urban growth onto major 2020 land-use/land-cover classes under SSP1–SSP3.

2020 LULC	Baseline area (km^2)	SSP1	SSP2	SSP3
Other cropland[1]	491.09	108.68 (22.1%)	125.49 (25.6%)	148.33 (30.2%)
Rice paddies	363.61	37.70 (10.4%)	50.86 (14.0%)	73.95 (20.3%)
Barren land	103.56	26.05 (25.1%)	32.66 (31.5%)	42.61 (41.1%)
Scrub/shrub	46.32	19.30 (41.7%)	21.61 (46.6%)	24.62 (53.2%)
Plantation trees	818.53	19.74 (2.4%)	25.70 (3.1%)	35.01 (4.3%)
Natural forest[2]	2550.34	10.04 (0.4%)	13.06 (0.5%)	18.01 (0.7%)
Aquaculture	68.31	4.80 (7.0%)	7.00 (10.2%)	10.89 (15.9%)
Grassland	21.55	2.24 (10.4%)	2.51 (11.6%)	2.88 (13.4%)
Mangrove	0.24	0.02 (10.3%)	0.03 (13.8%)	0.05 (19.5%)
Total (km^2)	—	**228.60**	**278.95**	**356.38**

Percentages in parentheses indicate the proportion of the respective 2020 land-use/land-cover class converted to simulated urban land by 2050. [1]Other cropland is a combination of woody crops and other croplands. [2]Natural Forest combines deciduous broadleaf, evergreen broadleaf, and evergreen needle-leaf forests. Open water recorded no simulated urban encroachment under any SSP because it was treated as a hard exclusion.

4.4. Changes in urban spatial configuration

The simulated urban landscapes showed substantial changes in spatial configuration between the 2020 baseline and 2050 across all three SSPs (Table 3). In 2020, the urban pattern comprised 14,780 patches, with a mean patch size (MPS) of 1.41 ha, a patch density (PD) of 2.95 patches per 100 ha, and a Landscape Shape Index (LSI) of 154.60. By 2050, all scenarios produced fewer and larger urban patches, indicating increasing aggregation and coalescence of the urban fabric.

The degree of coalescence increased from SSP1 to SSP3. Mean patch numbers declined from 6588 under SSP1–5675 under SSP2 and 4701 under SSP3, while MPS increased from 6.63 to 8.59 and 12.02 ha, respectively. PD decreased correspondingly from 1.32 to 1.13 and 0.94 patches per 100 ha. LSI also declined from 106.51 under SSP1–101.23 under SSP2 and 87.88 under SSP3, compared with 154.60 in 2020, indicating progressively simpler urban boundaries in the main

Table 3
Urban Landscape configuration for 2020 baseline and 2050 SSPs in Hue.

Metric	2020 baseline	SSP1	SSP2	SSP3
Number of patches	14,780	6588	5675	4701
Mean patch size (ha)	1.41	6.63	8.59	12.02
Patch density (patches/100 ha)	2.95	1.32	1.13	0.94
Landscape Shape Index	154.60	106.51	101.23	87.88

simulations. Paired comparisons using identical MC seeds showed that differences among SSPs exceeded stochastic variation for all four metrics. The corresponding 95% confidence intervals for the ensemble means and 5th–95th percentile ranges of the landscape metrics are reported in Table S11

The constant-area sensitivity analysis showed that part of the apparent coalescence was associated with differences in total urban growth quantity. Under equivalent growth quantities, the ordering of patch number, MPS, and PD changed. SSP3 produced more patches (7740), a lower MPS (5.65 ha), and a higher PD (1.55 patches per 100 ha) than SSP1 (7124 patches, 6.13 ha, and 1.42 patches per 100 ha), while SSP2 remained intermediate. This reversal indicates that the stronger coalescence observed in the main SSP3 simulation partly reflects its larger urban expansion, which increasingly fills gaps and connects previously separate urban areas.

LSI retained the same ordering under the constant-area comparison, decreasing from 86.84 under SSP1–81.72 under SSP2 and 75.02 under SSP3. This indicates that SSP3 produced comparatively simpler urban boundaries even when growth quantity was held constant. The sensitivity analysis therefore distinguishes two dimensions of future urban form: growth magnitude influences patch coalescence, while scenario-specific spatial allocation also shapes the distribution and boundary complexity of urban development.

4.5. Sensitivity of Simulated Urban Growth to Scenario Growth Settings and Spatial Protection

The controlled sensitivity experiments indicated that differences in simulated urban expansion among SSP1–SSP3 reflected the combined influence of growth settings and spatial protection assumptions. The common reference configuration, comprising the calibrated UGMr parameters and RF-plus-water resistance surface without additional SSP-specific protection, produced a mean 2050 urban extent of 553.87 km^2.

When the calibrated growth parameters were held constant and only the SSP-specific protection assumptions were varied, projected urban extent decreased by 89.7 km^2 under SSP1, 66.5 km^2 under SSP2, and 31.4 km^2 under SSP3 relative to the reference configuration. In contrast, varying only the growth settings while retaining the common RF-plus-water resistance surface reduced projected urban extent by 40.3 km^2 under SSP1 and increased it by 48.2 km^2 under SSP3. SSP2 retained the calibrated growth parameters and therefore showed no growth-setting effect relative to the reference configuration.

The combined effects of growth settings and spatial protection were not fully additive, with interaction terms of + 13.1 km^2 under SSP1 and −5.9 km^2 under SSP3. These findings demonstrate that differences in simulated urban extent reflected the combined effects of growth settings and spatial protection assumptions, including their interactions, within the specified scenario configurations.

5. Discussion

5.1. Urban Growth Magnitude under the different SSPs

The simulations indicate substantial urban expansion in Hue under all three locally downscaled SSPs, but with clear differences in magnitude. From a 2020 urban extent of 208.42 km^2, the mean simulated urban area reaches 437.02 km^2 under SSP1, 487.37 km^2 under SSP2, and 564.81 km^2 under SSP3 by 2050, corresponding to additional urban growth of 228.60, 278.95, and 356.38 km^2, respectively. The scenario ordering differs from many global and national SSP-based urban projections, where SSP1 or SSP2 can generate greater urban expansion than SSP3 owing to the slower economic and demographic growth generally associated with SSP3 (Gao & O'Neill, 2020; Jiang & O'Neill, 2017; Li et al., 2019; Zhuang et al., 2022). In Hue, the larger SSP3 urban footprint reflects the localized scenario assumptions, not greater economic prosperity. SSP3 combines higher land development pressure with weaker spatial protection, greater dispersion, and increased access to marginally suitable land. A resource constrained pathway can therefore remain spatially extensive where development consumes land inefficiently, peripheral areas become accessible, and restrictions on conversion are less strongly implemented.

The controlled sensitivity analysis also supports this distinction. When scenario-specific protection constraints were varied while the calibrated growth parameters were held constant, protection reduced the 2050 urban extent by approximately 89.7 km^2 under SSP1, 66.5 km^2 under SSP2, and 31.4 km^2 under SSP3 relative to the common RF-plus-water control. Conversely, varying only the growth parameters reduced the SSP1 urban extent by approximately 40.3 km^2 but increased SSP3 by approximately 48.2 km^2. Differences among the SSPs therefore arose from both the growth settings and the extent of spatial protection, with neither component accounting for the scenario divergence independently. This decomposition directly cautions against interpreting the larger SSP3 footprint as evidence that weak governance itself causes urban expansion; instead, the result follows from the interacting assumptions encoded in the localized scenario.

This result illustrates an important feature of local SSP operationalization. Downscaling does not require local urban area trajectories to reproduce global SSP rankings mechanically. Its value lies in retaining the broader logic of the pathways while explicitly translating locally relevant development pressures, planning conditions, and land protection priorities into spatial assumptions that can be examined transparently.

5.2. Spatial distribution and potential growth hotspots

Beyond differences in total urban extent, 29 hotspot clusters were identified under SSP1, 30 under SSP2, and 42 under SSP3, concentrated across recurring development zones in the coastal and low-lying areas, industrial and transport corridors, peripheral expansion around central Hue, lower plains adjoining mountainous terrain, and corridors extending toward the Laos border. These patterns suggest that future growth may intensify development processes already evident in these parts of Hue.

Coastal and low-lying development in Hue reflects a broader tension between locational advantage and environmental exposure. Across Asia, rapid coastal urbanization has concentrated population and assets in hazard prone areas, while continuing development increasingly coincides with climate related extremes (Aziz et al., 2024; Fox et al., 2024; Neumann et al., 2015; Wolff et al., 2020). Flooding remains one of the most damaging disaster types globally, with substantial populations and infrastructure already exposed to flood hazards (CRED & UNDRR., 2020; Rentschler et al., 2022). This tension is particularly relevant in Hue, where coastal and lagoon areas support fisheries, tourism, settlement, and other livelihood activities while also providing important ecosystem functions and opportunities for EbA (Cao et al., 2024; Phuong et al., 2023; Tuan, 2022). The simulations indicate that future development pressure may remain spatially aligned with areas already identified as flood-prone, illustrating the planning challenge of accommodating development while maintaining environmentally sensitive land. As the flood layer represents historically identified flood-prone land, the simulations indicate potential spatial overlap with existing flood-prone areas, not future flood risk.

The concentration of projected growth around industrial corridors is also consistent with Hue's ongoing economic restructuring, in which construction and industrial activities have become increasingly important components of the local economy (Hang, 2024). Comparable patterns have been reported in other studies where industrial zones and associated infrastructure can stimulate surrounding urban expansion (Haldar et al., 2024; Qiu et al., 2015). Such corridors can attract residential and commercial development through employment, road accessibility, and infrastructure provision, creating additional pressure on neighboring peri-urban and agricultural land.

The model results also indicate possible continued outward expansion beyond central Hue. This trend is consistent with recent observations that existing urban development is extending into peripheral areas, particularly toward the east and south, where new residential development has occurred on former paddy fields (Linh et al., 2024). The model therefore reproduces a spatial tendency already visible in the contemporary urbanization process rather than introducing an entirely new direction of urbanization. Also, western development toward the Laos border is consistent with the wider role of the East–West Economic Corridor in strengthening mobility and economic interaction between Vietnam and Laos (Nonthapot et al., 2019). International evidence also shows that transport infrastructure and cross-border economic linkages can influence settlement development in border regions (Wang et al., 2018; Zhao et al., 2017). In Hue, improved accessibility toward the western part of the province could therefore create new development opportunities, although the model does not independently establish cross-border migration or infrastructure investment as causal drivers. Rather, the spatial pattern is consistent with these wider regional development processes.

These spatial differences call for location-specific planning responses: risk-sensitive development control and retention of flood-storage land in coastal lowlands; coordinated residential and industrial land management along economic corridors; protection of peri-urban agricultural buffers around expanding settlements; and ecological and slope safeguards where new infrastructure opens western and mountainous development fronts.

5.3. Future urban encroachment on other land use types in Hue

Urban expansion frequently occurs through the conversion of existing non-urban land uses (Liu et al., 2021; McManamay et al., 2024; Sharma et al., 2024), making the type of land displaced by future development an important dimension of urban sustainability. The strong pressure on agricultural land in Hue is consistent with regional and global projections identifying cropland as a major source of land for future urban development (Chen et al., 2020; Doelman et al., 2018; Popp et al., 2017; Zhuang et al., 2022). Peri-urban agricultural land is particularly susceptible to conversion where relatively flat terrain, accessibility, and proximity to existing development facilitate urban expansion. The significance of this conversion extends beyond the amount of land lost. Rice fields and other cultivated landscapes support local production and peri-urban livelihoods (Phục et al., 2025), while also providing multifunctional landscape and ecosystem services, including water storage and runoff regulation (Lee et al., 2015). Their conversion can therefore increase competition between urban development, agricultural livelihoods, and the retention of land that may contribute to environmental and adaptation functions.

Pressure on plantation land, shrubland, aquaculture, and other open landscapes points to a broader conflict between urban expansion and ecological or productive functions. Yang et al. (2022) documented losses of wetland ecosystem services associated with the expansion of impervious surfaces, while Mao et al. (2021) identified urban encroachment affecting wetland related ecosystems, including shrubland, within a Ramsar landscape in China. Mrozik et al. (2019) similarly demonstrated conflicts between peri-urban expansion and aquaculture in Bangkok. These studies show that conversion impacts may extend beyond agricultural production to ecological functions and livelihood systems relevant to adaptation planning.

The distinction between absolute and proportional conversion is also important for land management. Extensive agricultural classes can experience the greatest total loss, while smaller land-cover classes may face greater proportional pressure. Natural forests may show limited proportional conversion at the landscape scale, while localized losses remain important where they affect ecological connectivity or strategically important conservation areas. Planning priorities should therefore consider both the quantity of land converted and the relative scarcity or functional importance of the affected land-use class.

5.4. Spatial distribution and pattern under different SSPs

The landscape analysis shows that differences in urban form reflect both growth quantity and spatial allocation. The greater coalescence apparent in the main SSP3 simulation partly results from its larger amount of development, which creates more opportunities for new growth to fill gaps and connect existing urban patches. The constant area sensitivity changes this interpretation: under equivalent growth quantities, SSP3 generates more numerous and smaller patches than SSP1, indicating a more dispersed allocation of development.

Dispersed peripheral expansion has been associated with development environments characterized by high land-development pressure and weaker control over peripheral growth (Jia et al., 2019; Shen et al., 2022). Planning and institutional conditions can also influence the spatial organization of urban development (Fertner et al., 2016). These comparisons support the plausibility of the scenario differences, while the present analysis does not isolate governance as an independent causal determinant of urban form.

Boundary complexity provides an additional distinction. LSI remains lower under SSP3 even when growth quantity is controlled, indicating that greater dispersion does not necessarily imply more irregular patch boundaries. Patch coalescence, dispersion, and boundary complexity therefore represent different dimensions of urban form and should not be interpreted interchangeably when comparing SSP-based urban futures.

5.5. Methodological contribution, Planning implications, Limitation, and Transferability

The principal methodological contribution lies in the operationalization of locally downscaled SSP narratives within an empirically informed urban growth framework. Participatory scenario development is linked with RF-derived growth propensity, scenario-specific spatial protection, stochastic UGMr simulation, and controlled sensitivity testing. This sequence makes explicit how qualitative assumptions are converted into spatial model inputs while retaining historical development patterns as an empirical constraint.

The sensitivity analyses strengthen the interpretation of the scenario comparisons. Protection and growth setting experiments demonstrate that scenario divergence reflects both components and that their effects can partially offset each other. The constant-area analysis further shows that differences in apparent urban form depend partly on the quantity of development simulated. These diagnostics are important given that varying growth and protection assumptions simultaneously could otherwise make their individual contributions difficult to distinguish. Therefore, the resulting SSPs should be interpreted as an internally consistent conditional pathway.

The spatial diversity of projected growth across Hue implies that planning responses should be tailored to the environmental and development pressures of different parts of the province. In coastal and lagoon lowlands, this means combining risk-sensitive zoning with protection of land important for agriculture, aquaculture, ecosystem functions, and flood management, while growth along industrial and transport corridors requires tighter coordination to limit ribbon development and loss of productive peri-urban land. Around central Hue and planned satellite settlements, development should be coordinated with infrastructure provision and broader spatial planning to avoid poorly connected peripheral expansion. In the mountainous and western parts of Hue, including corridors toward the Laos border, future development should account for slope constraints and the ecological sensitivity of surrounding land.

Several limitations define the scope of the findings. Expert-derived protection assumptions were informed by a small purposively selected group, so the scenario parameters reflect a bounded range of local

expertise and retain elicitation uncertainty. The same participants contributed to the subsequent plausibility assessment, which was used to assess the internal consistency and contextual plausibility of the simulated spatial patterns. The flood layer represents historically identified flood-prone land and does not incorporate future changes in rainfall, sea level, river discharge, or flood defenses; consequently, simulated development in these areas indicates potential spatial conflict with existing flood-prone land, not future flood risk. The 30-m JAXA data limit interpretation of fine-scale land-use transitions, while the protection allocation represents scenario-specific protection proportions without identifying the exact locations that may receive future protection. The analysis was also restricted to SSP1–SSP3, reflecting the study context, Vietnam's adaptation priorities, and local expert judgement (Vu, Obaitor, Katzschner, et al., 2025).

These limitations also define the conditions for applying the framework beyond Hue. Its transferable contribution is the workflow for translating locally grounded SSP assumptions into spatially explicit urban growth pathways, while development drivers, scenario assumptions, protection priorities, and UGMr settings require local specification. The remaining uncertainties also point to opportunities for extending the framework. Coupling SSPs with corresponding climate-forcing pathways could examine interactions among urbanization, climate change, and flood exposure, while linking alternative urban forms with hydrological modelling could clarify how the amount and spatial configuration of future development influence flood processes in coastal cities.

6. Conclusion

This study develops a locally grounded workflow for translating downscaled Shared Socioeconomic Pathways into spatially explicit urban growth scenarios. The framework integrates participatory scenario development, Random Forest-derived growth propensity, scenario-specific spatial protection, and stochastic urban growth simulation, providing a transparent way to operationalize qualitative SSP narratives within a quantitative modeling framework. This framework was operationalized in Hue, Vietnam.

The simulations produced clearly differentiated urban futures across SSP1–SSP3, with urban expansion increasing progressively from SSP1 to SSP3 and concentrating along coastal and lagoon areas, transport and industrial corridors, peripheral areas around central Hue, and western development fronts. These trajectories were accompanied by increasing conversion of agricultural and other non-urban land, with cropland and rice fields accounting for much of the projected land-use change. Urban form also differed across scenarios: greater expansion promoted stronger patch coalescence, while the constant-area analysis showed that spatial allocation continued to shape patch number, size, density, and boundary configuration independently of growth quantity. Sensitivity experiments further showed that both scenario-specific growth settings and spatial protection assumptions contributed to differences among the SSP outcomes. The findings therefore demonstrate that future urban form in Hue is shaped not only by how much development occurs but also by where development is directed and which landscapes are protected. The resulting SSP simulations provide conditional spatial pathways for examining these interacting development and land-management choices. The framework therefore provides a transferable way to link locally grounded socioeconomic pathways, empirical urban growth modelling, and spatial planning constraints for examining alternative urban futures under uncertainty.

CRediT authorship contribution statement

Olabisi S. Badmos: Writing – review & editing, Writing – original draft, Validation, Software, Methodology, Investigation, Formal analysis, Data curation, Conceptualization. **Oluwafemi M. Odunsi:** Writing – review & editing, Writing – original draft. **Andrea Ortiz Vargas:** Writing – review & editing. **Bien Thanh Vu:** Writing – review & editing, Investigation. **Lena C. Grobusch:** Writing – review & editing. **Antje Katzschner:** Writing – review & editing. **Linh Nguyen Hoang Khanh:** Writing – review & editing. **Volker Hochschild:** Writing – review & editing, Funding acquisition. **Felix Bachofer:** Writing – review & editing, Funding acquisition. **Matthias Garschagen:** Writing – review & editing, Project administration, Funding acquisition, Conceptualization.

Declaration of Generative AI and AI-assisted technologies in the writing process

During the preparation of this work, the authors used QuillBot to improve the language and readability of the text. After using this tool, the authors reviewed and edited the content as needed and take full responsibility for the content of the published article.

Funding

This research was part of the FloodAdaptVN project, funded by the German Federal Ministry of Research, Technology, and Space (BMFTR) through its Research for Sustainable Development (FONA) program and the Sustainable Development of Urban Regions (SURE) funding priority (Grant Numbers: 01LE1905F1, 01LE1905A1).

Declaration of Competing Interest

The authors declare that they have no known competing financial interests or personal relationships that could have appeared to influence the work reported in this paper.

Appendix A. Supporting information

Supplementary data associated with this article can be found in the online version at doi:10.1016/j.landusepol.2026.108431.

Data availability

Data will be made available on request.

References

Aziz, F., Wang, X., Mahmood, M.Q., Awais, M., Trenouth, B., 2024. Coastal urban flood risk management: Challenges and opportunities– A systematic review. J. Hydrol., 132271

Bachofer, F., Wang, Z., Huth, J., Eisfelder, C., Reimuth, A., Kuenzer, C., 2026. Urban growth prediction along Shared Socioeconomic Pathways (SSPs) for future flood exposure risk assessment: A cross-continental analysis of coastal cities. Anthr. Coasts 9 (1), 1. https://doi.org/10.1007/s44218-025-00109-6.

Badmos, O.S., Rienow, A., Callo-Concha, D., Greve, K., Jürgens, C., 2019. Simulating slum growth in Lagos: An integration of rule based and empirical based model. Comput. Environ. Urban. Syst. 77, 101369. https://doi.org/10.1016/j.compenvurbsys.2019.101369.

Bhusal, K., Udas, E., Bhatta, L.D., 2022. Ecosystem-based adaptation for increased agricultural productivity by smallholder farmers in Nepal. PLOS ONE 17 (6), e0269586. https://doi.org/10.1371/journal.pone.0269586.

Breiman, L., 2001. Random Forests. Mach. Learn. 45 (1), 5–32. https://doi.org/10.1023/A:1010933404324.

Cao, T.T., Truong Van, T., Le Phi Ho, K., 2024. When tourism intersects traditional rural livelihoods: A case study on lagoon fishing in Thừa Thiên Huế Province, Vietnam. Community Dev. 55 (5), 775–787. https://doi.org/10.1080/15575330.2024.2356675.

Carlino, G.A., Saiz, A., 2019. Beautiful city: Leisure amenities and urban growth. J. Reg. Sci. 59 (3), 369–408. https://doi.org/10.1111/jors.12438.

CBD. (2009). Connecting Biodiversity and Climate Change Mitigation and Adaptation: Report of the Second Ad Hoc Technical Expert Group on Biodiversity and Climate Change. Secretariat of the Convention on Biological Diversity.

Chaudhry, P., & Ruysschaert, G. (2008). Climate Change and Human Development in Viet Nam Peter Chaudhry and Greet Ruysschaert. Undp.

Chen, G., Li, X., Liu, X., Chen, Y., Liang, X., Leng, J., Huang, K., 2020. Global projections of future urban land expansion under shared socioeconomic pathways. Nat. Commun. 11 (1), 537. https://doi.org/10.1038/s41467-020-14386-x.

Chen, Y., Li, X., Liu, X., Zhang, Y., Huang, M., 2019. Tele-connecting China's future urban growth to impacts on ecosystem services under the shared socioeconomic

pathways. Sci. Total. Environ. 652, 765–779. https://doi.org/10.1016/j.scitotenv.2018.10.283.
Cheng, Y., Kang, Q., Liu, K., Cui, P., Zhao, K., Li, J., Ma, X., Ni, Q., 2023. Impact of Urbanization on Ecosystem Service Value from the Perspective of Spatio-Temporal Heterogeneity: A Case Study from the Yellow River Basin. Land 12 (7), 1301. https://doi.org/10.3390/land12071301.
Clarke, K.C., 2008. Mapping and Modelling Land Use Change: An Application of the SLEUTH Model. In: Pettit, In.C., Cartwright, W., Bishop, I., Lowell, K., Pullar, D., Duncan, D. (Eds.), Landscape Analysis and Visualisation: Spatial Models for Natural Resource Management and Planning. Springer, pp. 353–366. https://doi.org/10.1007/978-3-540-69168-6_17.
Clarke, K.C., Hoppen, S., Gaydos, L., 1997. A Self-Modifying Cellular Automaton Model of Historical Urbanization in the San Francisco Bay Area. Environ. Plan. B Plan. Des. 24 (2), 247–261. https://doi.org/10.1068/b240247.
CRED, UNDRR, 2020. Human. Cost. Disaster. Overv. Last 20 Years. https://www.undrr.org/publication/human-cost-disasters-overview-last-20-years-2000-2019.
D'Amour, C.B., Reitsma, F., Baiocchi, G., Barthel, S., Güneralp, B., Erb, K.H., Haberl, H., Creutzig, F., Seto, K.C., 2017. Future urban land expansion and implications for global croplands. Proc. Natl. Acad. Sci. USA 114 (34), 8939–8944. https://doi.org/10.1073/pnas.1606036114.
Doelman, J.C., Stehfest, E., Tabeau, A., Meijl, H., Lassaletta, L., Gernaat, D.E., Vuuren, D. P., 2018. Exploring SSP land-use dynamics using the IMAGE model: Regional and gridded scenarios of land-use change and land-based climate change mitigation. Glob. Environ. Change 48, 119–135. https://doi.org/10.1016/j.gloenvcha.2017.11.014.
Fertner, C., Jørgensen, G., Nielsen, T.A.S., Nilsson, K.S.B., 2016. Urban sprawl and growth management – drivers, impacts and responses in selected European and US cities. Future Cities Environ. 2 (1), 9. https://doi.org/10.1186/s40984-016-0022-2.
Fox, S., Agyemang, F., Hawker, L., Neal, J., 2024. Integrating social vulnerability into high-resolution global flood risk mapping. Nat. Commun. 15 (1), 3155. https://doi.org/10.1038/s41467-024-47394-2.
Gao, J., O'Neill, B.C., 2020. Mapping global urban land for the 21st century with data-driven simulations and Shared Socioeconomic Pathways. Nat. Commun. 11 (1), 1–12. https://doi.org/10.1038/s41467-020-15788-7.
Garschagen, M., Romero-Lankao, P., 2015. Exploring the relationships between urbanization trends and climate change vulnerability. Clim. Change 133 (1), 37–52. https://doi.org/10.1007/s10584-013-0812-6.
Goetzke, R. (2011). Entwicklung eines fernerkundungsgestützten Modellverbundes zur Simulation des urban-ruralen Landnutzungswandels in Nordrhein-Westfalen. Verlag. http://hss.ulb.uni-bonn.de/2011/2577/2577.htm.
González, C., Bachmann, M., Bueso-Bello, J.-L., Rizzoli, P., Zink, M., 2020. A Fully Automatic Algorithm for Editing the TanDEM-X Global DEM. Article 23. Remote. Sens. 12 (23). https://doi.org/10.3390/rs12233961.
Güneralp, B., Seto, K.C., 2013. Futures of global urban expansion: Uncertainties and implications for biodiversity conservation. Environ. Res. Lett. 8 (1), 014025. https://doi.org/10.1088/1748-9326/8/1/014025.
Haldar, S., Chatterjee, U., Bhattacharya, S., Paul, S., Bindajam, A.A., Mallick, J., Abdo, H. G., 2024. Peri-urban dynamics: Assessing expansion patterns and influencing factors. Ecol. Process. 13 (1), 58. https://doi.org/10.1186/s13717-024-00533-5.
Hallegatte, S., Green, C., Nicholls, R.J., Corfee-Morlot, J., 2013. Future flood losses in major coastal cities. Nat. Clim. Change 3 (9), 802–806. https://doi.org/10.1038/nclimate1979.
Hang, L.V. (2024). Thua Thien Hue: An Emerging Investment Destination. Vietnam Briefing. https://www.vietnam-briefing.com/news/thua-thien-hue-an-emerging-investment-destination.html/.
He, W., Li, X., Zhou, Y., Shi, Z., Yu, G., Hu, T., Wang, Y., Huang, J., Bai, T., Sun, Z., Liu, X., Gong, P., 2023. Global urban fractional changes at a 1 km resolution throughout 2100 under eight scenarios of Shared Socioeconomic Pathways (SSPs) and Representative Concentration Pathways (RCPs). Earth Syst. Sci. Data 15 (8), 3623–3639. https://doi.org/10.5194/essd-15-3623-2023.
Herold, M., Couclelis, H., Clarke, K.C., 2005. The role of spatial metrics in the analysis and modeling of urban land use change. Comput. Environ. Urban. Syst. 29 (4), 369–399. https://doi.org/10.1016/j.compenvurbsys.2003.12.001.
Hoang Nam, B., Le Van, N., Hoang Vu, H., 2024. Applications of satellite data for rapid inundation assessment—A case study in Thua Thien Hue province. Transp. Commun. Sci. J. 75 (4), 1697–1706. https://doi.org/10.47869/tcsj.75.4.18.
Hou, Y., Li, Y., Li, J., Huang, Q., Duan, X., Feng, X., Zhu, G., 2023. Simulating the dynamics of urban land quantity in China from 2020 to 2070 under the Shared Socioeconomic Pathways. Appl. Geogr. 159, 103094. https://doi.org/10.1016/j.apgeog.2023.103094.
Huang, M., Wang, Z., Pan, X., Gong, B., Tu, M., Liu, Z., 2022. Delimiting China's Urban Growth Boundaries Under Localized Shared Socioeconomic Pathways and Various Urban Expansion Modes. Earth'S. Future 10 (6), e2021EF002572. https://doi.org/10.1029/2021EF002572.
Hue Statistics Office. (2022). Statistical yearbook Thanh Pho Hue 2021. General Statistics Office of Vietnam.
Huong, H.T.L., Pathirana, A., 2013. Urbanization and Climate Change Impacts on Future Urban Flooding in Can Tho City, Vietnam. Hydrol. Earth Syst. Sci. 17 (1), 379–394. https://doi.org/10.5194/hess-17-379-2013.
IPCC, 2023. Climate Change 2023 Synthesis Report. Contribution Working Groups I II III Sixth Assessment Report Intergovernmental Panel Climate Change 184. https://doi.org/10.59327/IPCC/AR6-9789291691647 (Intergovernmental Panel on Climate Change (IPCC)).
Jantz, C.A., Goetz, S.J., Donato, D., Claggett, P., 2010. Designing and implementing a regional urban modeling system using the SLEUTH cellular urban model. Comput. Environ. Urban. Syst. 34 (1), 1–16. https://doi.org/10.1016/j.compenvurbsys.2009.08.003.
Japan Aerospace Exploration Agency (JAXA), 2021. Annual land-use and land-cover maps across mainland Vietnam from 1990 to 2020 (Version 21.09, Level 2). Earth Observation Research Center (EORC). Japan Aerospace Exploration Agency. https://www.eorc.jaxa.jp/ALOS/en/dataset/lulc/lulc_vnm_v2109_e.htm [Dataset].
Jia, Y., Tang, L., Xu, M., Yang, X., 2019. Landscape pattern indices for evaluating urban spatial morphology – A case study of Chinese cities. Ecol. Indic. 99, 27–37. https://doi.org/10.1016/j.ecolind.2018.12.007.
Jiang, L., O'Neill, B.C., 2017. Global urbanization projections for the Shared Socioeconomic Pathways. Glob. Environ. Change 42, 193–199. https://doi.org/10.1016/j.gloenvcha.2015.03.008.
Lee, Y.-C., Ahern, J., Yeh, C.-T., 2015. Ecosystem services in peri-urban landscapes: The effects of agricultural landscape change on ecosystem services in Taiwan's western coastal plain. Landsc. Urban. Plan. 139, 137–148. https://doi.org/10.1016/j.landurbplan.2015.02.023.
Li, S., Zhou, C., Wang, S., Gao, S., Liu, Z., 2019. Spatial heterogeneity in the determinants of urban form: An analysis of Chinese cities with a GWR approach. Sustain. (Switz.) 11 (2). https://doi.org/10.3390/su11020479.
Linh, N.H.K., Pham, T.G., Pham, T.H., Tran, C.T.M., Nguyen, T.Q., Ha, N.T., Ngoc, N.B., 2024. Land-Use and Land-Cover Changes and Urban Expansion in Central Vietnam: A Case Study in Hue City. Urban. Sci. 8, 242. https://doi.org/10.3390/urbansci8040242.
Liu, S., Zhang, J., Geng, Y., Li, J., Wang, Y., Zhang, J., 2021. Plausible response of urban encroachment on ecological land to tourism growth and implications for sustainable management, a case study of Zhangjiajie, China. Ecol. Indic. 132, 108253. https://doi.org/10.1016/j.ecolind.2021.108253.
Liu, Y., Li, L., Chen, L., Cheng, L., Zhou, X., Cui, Y., Li, H., Liu, W., 2019. Urban growth simulation in different scenarios using the SLEUTH model: A case study of Hefei, East China. PLOS ONE 14 (11), e0224998. https://doi.org/10.1371/journal.pone.0224998.
Liu, Y., Yang, M., Cui, J., 2024. Urbanization, economic agglomeration and economic growth. e23772 Heliyon 10 (1). https://doi.org/10.1016/j.heliyon.2023.e23772.
Magnan, A.K., Oppenheimer, M., Garschagen, M., Buchanan, M.K., Duvat, V.K.E., Forbes, D.L., Ford, J.D., Lambert, E., Petzold, J., Renaud, F.G., Sebesvari, Z., van de Wal, R.S.W., Hinkel, J., Pörtner, H.-O., 2022. Sea level rise risks and societal adaptation benefits in low-lying coastal areas. Sci. Rep. 12 (1), 10677. https://doi.org/10.1038/s41598-022-14303-w.
Mao, D., Wang, Z., Wang, Y., Choi, C., Jia, M., Jackson, M., Fuller, R., 2021. Remote observations in china's ramsar sites: Wetland dynamics, anthropogenic threats, and implications for sustainable development goals. J. Remote. Sens. https://doi.org/10.34133/2021/9849343.
McGarigal, K., & Marks, B.J. (1995). FRAGSTATS: Spatial pattern analysis program for quantifying landscape structure. (PNW-GTR-351; p. PNW-GTR-351). U.S. Department of Agriculture, Forest Service, Pacific Northwest Research Station. https://doi.org/10.2737/PNW-GTR-351.
McManamay, R.A., Raad, A., Vernon, C.R., Thurber, T., Gao, J., Powers, S., O'Neill, B., 2024. Divergent urban land trajectories under alternative population projections within the Shared Socioeconomic Pathways. Environ. Res. Lett. 19 (4). https://doi.org/10.1088/1748-9326/ad2eec.
Mercado, M.J.T., Garcia, J.N.M., Calalo, F.C., Sobremisana, M.J., Olvida, I., de, G., Revilla, G., 2023. Exploring Ecosystem-Based Adaptation (EbA) as climate change adaptation strategy in brgy. Bagupaye, Mulanay, Quezon, Philippines. South. Fla. J. Dev. 4 (5), 2079–2090. https://doi.org/10.46932/sfjdv4n5-019.
Mills, A.J., Tan, D., Manji, A.K., Vijitpan, T., Henriette, E., Murugaiyan, P., Pantha, R.H., Lafdal, M.Y., Soule, A., Cazzetta, S., Bégat, P., Vlieghe, K.E.P., Lavirotte, L., Kok, J.T., Lister, J., 2020. Ecosystem-based adaptation to climate change: Lessons learned from a pioneering project spanning Mauritania, Nepal, the Seychelles, and China. PLANTS PEOPLE PLANET 2 (6), 587–597. https://doi.org/10.1002/ppp3.10126.
Mrozik, W., Vinitnantharat, S., Thongsamer, T., Pansuk, N., Pattanachan, P., Thayanukul, P., Werner, D., 2019. The food-water quality nexus in periurban aquacultures downstream of bangkok, thailand. Sci. Total. Environ. 695, 133923. https://doi.org/10.1016/j.scitotenv.2019.133923.
Mubea, K., Menz, G., 2014. Evaluation of a self-modifying cellular automata in modelling urban growth in Nyeri (Kenya). Int. J. Technol. Enhanc. Emerg. Eng. Res. 3 (12), 177–183.
Muneer, H., 2023. The Impact of Urbanization on the Environment. Lib. J. Lang. & Lit. Rev. 1 (01), 45–54.
Nehren, U., Ho Dac, H., Raedig, C., & Alfonso de Nehren, S. (2017). Sand Dunes and Mangroves for Disaster Risk Reduction and Climate Change Adaptation in the Coastal Zone of Quang Nam Province, Vietnam. https://doi.org/10.1007/978-981-10-2624-9_13.
Neumann, B., Vafeidis, A.T., Zimmermann, J., Nicholls, R.J., 2015. Future Coastal Population Growth and Exposure to Sea-Level Rise and Coastal Flooding—A Global Assessment. PLoS. ONE 10 (3).
Nonthapot, S., Dinh, T.N., Thuan, Y.T., 2019. The process of land passenger transportation by international bus crossing Lao and Vietnamese border gates. Open. Transp. J. 13 (1). https://doi.org/10.2174/1874447801913010001.
O'Neill, B.C., Kriegler, E., Ebi, K.L., Kemp-Benedict, E., Riahi, K., Rothman, D.S., van Ruijven, B.J., van Vuuren, D.P., Birkmann, J., Kok, K., Levy, M., Solecki, W., 2017. The roads ahead: Narratives for shared socioeconomic pathways describing world futures in the 21st century. Glob. Environ. Change 42, 169–180. https://doi.org/10.1016/j.gloenvcha.2015.01.004.
O'Neill, B.C., Kriegler, E., Riahi, K., Ebi, K.L., Hallegatte, S., Carter, T.R., Mathur, R., van Vuuren, D.P., 2014. A new scenario framework for climate change research: The

concept of shared socioeconomic pathways. Clim. Change 122 (3), 387–400. https://doi.org/10.1007/s10584-013-0905-2.
Obaitor, O.S., Odunsi, O.M., Vu, T.B., Grobusch, L.C., Schultz, M., Hochschild, V., Khanh, L.N.H., Garschagen, M., 2025. Spatial Dynamics and Drivers of Urban Growth in Thua Thien Hue Province, Vietnam: Insights for Urban Sustainability in the Global South. Article 2. ISPRS Int. J. Geo-Inf. 14 (2). https://doi.org/10.3390/ijgi14020044.
Palmer, D., Wehrmann, B., & Fricska, S. (2009). Towards improved land governance. UN-HABITAT. https://openknowledge.fao.org/server/api/core/bitstreams/61349153-20d8-4802-86d5-ccfa15550e5e/content.
Phan, D.C., Trung, T.H., Truong, V.T., Sasagawa, T., Vu, T.P.T., Bui, D.T., Hayashi, M., Tadono, T., Nasahara, K.N., 2021. First comprehensive quantification of annual land use/cover from 1990 to 2020 across mainland Vietnam. Sci. Rep. 11 (1), 9979. https://doi.org/10.1038/s41598-021-89034-5. https://www.nature.com/articles/s41598-021-89034-5. (Accessed 11 May 2021).
Phục, N.Q., Hà, T.A., Hương, H.T.T., Quý, N.P.B., 2025. CHIẾN LƯỢC SINH KẾ CỦA HỘ NÔNG DÂN VÙNG VEN THÀNH PHỐ HUẾ TRONG BỐI CẢNH ĐÔ THỊ HOÁ. Hue University Journal Science Economics Development 134 (5C), 5–15. https://doi.org/10.26459/hueunijed.v134i5C.8003.
Phuong, L.T.H., Thắng, T.Q., Yến, H.H., Hằng, Đ.T., 2023. ĐÁNH GIÁ KẾT QUẢ CÁC GIẢI PHÁP THÍCH ỨNG VỚI BIẾN ĐỔI KHÍ HẬU DỰA VÀO HỆ SINH THÁI (EbA) TRONG LĨNH VỰC NÔNG NGHIỆP TẠI HỆ ĐẦM PHÁ TAM GIANG-CẦU HAI, TỈNH THỪA THIÊN HUẾ. Hue University Journal Science Agriculture Rural Development 132 (3D). https://doi.org/10.26459/hueunijard.v132i3D.7292.
Phuong, T.T., Tan, N.Q., Dinh, N.C., Van Chuong, H., Ha, H.D., Hung, H.T., 2023. Livelihood vulnerability to climate change: Indexes and insights from two ethnic minority communities in Central Vietnam. Environ. Chall. 10, 100666. https://doi.org/10.1016/j.envc.2022.100666.
Popp, A., Calvin, K., Fujimori, S., Havlik, P., Humpenöder, F., Stehfest, E., Vuuren, D.P., 2017. Land-use futures in the shared socio-economic pathways. Glob. Environ. Change 42, 331–345. https://doi.org/10.1016/j.gloenvcha.2016.10.002.
Qiu, R., Xu, W., Zhang, J., 2015. The transformation of urban industrial land use: A quantitative method. J. Urban. Manag. 4 (1), 40–52. https://doi.org/10.1016/j.jum.2015.07.001.
Reimann, L., Vafeidis, A.T., Honsel, L.E., 2023. Population development as a driver of coastal risk: Current trends and future pathways. Camb. Prism. Coast. Futures 1, e14. https://doi.org/10.1017/cft.2023.3.
Rentschler, J., Salhab, M., Jafino, B.A., 2022. Flood exposure and poverty in 188 countries. Nat. Commun. 13 (1), 3527. https://doi.org/10.1038/s41467-022-30727-4.
Rienow, A., Goetzke, R., 2015. Supporting SLEUTH – Enhancing a cellular automaton with support vector machines for urban growth modeling. Comput. Environ. Urban. Syst. 49, 66–81. https://doi.org/10.1016/j.compenvurbsys.2014.05.001.
Schmitz, M., Bode, T., Thamm, H.P., Cremers, A.B., 2007. XULU - A generic JAVA-based platform to simulate land use and land cover change (LUCC). In: Oxley, L., Kulasiri, D. (Eds.), MODSIM 2007 International Congress on Modelling and Simulation. Modelling and Simulation Society of Australia, New Zealand, pp. 2645–2649. https://doi.org/10.1117/1.JRS.11.035015.
Seto, K.C., Fragkias, M., Güneralp, B., Reilly, M.K., 2011. A Meta-Analysis of Global Urban Land Expansion. e23777–e23777 PLoS. ONE 6 (8). https://doi.org/10.1371/journal.pone.0023777.
Seto, K.C., Güneralp, B., Hutyra, L.R., 2012. Global forecasts of urban expansion to 2030 and direct impacts on biodiversity and carbon pools. Proc. Natl. Acad. Sci. USA 109 (40), 16083–16088. https://doi.org/10.1073/pnas.1211658109.
Sett, D., Trinh, T.P., Wasim, T., Ortiz-Vargas, A., Nguyen, D.G.C., Büche, K., Assmann, A., Nguyen, H.K.L., Walz, Y., Souvignet, M., Bachofer, F., Vu, T.B., Garschagen, M., Hagenlocher, M., 2024. Advancing understanding of the complex nature of flood risks to inform comprehensive risk management: Findings from an urban region in Central Vietnam. Int. J. Disaster Risk Reduct. 110, 104652. https://doi.org/10.1016/j.ijdrr.2024.104652.
Sharma, M., Kumar, V., Kumar, S., 2024. A systematic review of urban sprawl and land use/land cover change studies in India. Sustain. Environ. 10 (1), 2331269. https://doi.org/10.1080/27658511.2024.2331269.
Shen, X., Wang, J., Zhang, X., Bei, H., 2022. Review of Research on Non-Conforming Urban Expansion: Measurement, Interpretation, and Governance. Land 11 (12), 2110. https://doi.org/10.3390/land11122110.
Siabi, E.K., Kabo-bah, A.T., Anornu, G., Akpoti, K., Mortey, E.M., Manson Incoom, A.B., Yeboah, K.A., 2025. Future land use simulation modeling for sustainable urban development under the shared socioeconomic pathways in West African megacities: Insights from Greater Accra Region. J. Environ. Manag. 376, 124300. https://doi.org/10.1016/j.jenvman.2025.124300.
Trung Thanh, H., Tschakert, P., Hipsey, M.R., 2021. Moving up or going under? Differential livelihood trajectories in coastal communities in Vietnam. World Dev. 138, 105219. https://doi.org/10.1016/j.worlddev.2020.105219.
TTH. (2023, December 30). Thừa Thiên Huế Province Planning for the Period 2021—2030, Vision to 2050. THƯ VIỆN PHÁP LUẬT. https://thuvienphapluat.vn/van-ban/Xay-dung-Do-thi/Quyet-dinh-1745-QD-TTg-2023-phe-duyet-Quy-hoach-tinh-Thua-Thien-Hue-thoi-ky-2021-2030-594454.aspx.
Tuan, N.T., 2022. Urbanization and land use change: A study in Vietnam. Environ. Socio-Econ. Stud. 10 (2), 19–29. https://doi.org/10.2478/environ-2022-0008.
Udessa, F., 2024. Urban land governance: Towards a conceptual framework. J. Geogr. Reg. Plan. 17 (3), 46–62.
UN-Habitat. (2022). World Cities Report 2022: Envisaging the Future of Cities. United Nations Human Settlements Programme.
UNDESA. (2018). World urbanization prospects: The 2018 revision. United Nations. https://population.un.org/wup/assets/WUP2018-Report.pdf.
van Vuuren, D.P., Kriegler, E., O'Neill, B.C., Ebi, K.L., Riahi, K., Carter, T.R., Edmonds, J., Hallegatte, S., Kram, T., Mathur, R., Winkler, H., 2014. A new scenario framework for Climate Change Research: Scenario matrix architecture. Clim. Change 122 (3), 373–386. https://doi.org/10.1007/s10584-013-0906-1.
Verma, A., Das, P., 2024. Urbanization in the Global South: Perspectives and Challenges. Vikalpa J. Decis. Mak. 49 (1), 110–112. https://doi.org/10.1177/02560909241234200.
Vu, B.T., Obaitor, O.S., Grobusch, L.C., Sett, D., Hagenlocher, M., Schinkel, U., Hoang Nguyen, L.K., Bachofer, F., Ngo, S.T., Garschagen, M., 2025. Enablers and barriers to implementing effective disaster risk management according to good governance principles: Lessons from Central Vietnam. Int. J. Disaster Risk Reduct. 120, 105344. https://doi.org/10.1016/j.ijdrr.2025.105344.
Vu, B.T., Obaitor, O.S., Katzschner, A., Grobusch, L.C., Sett, D., Ortiz-Vargas, A., Hagenlocher, M., Schinkel, U., Bachofer, F., Nguyen, L.K.H., Garschagen, M., 2025. A novel approach to developing local flood vulnerability scenarios based on the Shared Socioeconomic Pathways framework: Sectoral risks and policy implications. Glob. Environ. Change 95, 103079. https://doi.org/10.1016/j.gloenvcha.2025.103079.
Wamsler, C., 2015. Mainstreaming ecosystem-based adaptation: Transformation toward sustainability in urban governance and planning. Ecol. Soc. 20 (2). https://www.jstor.org/stable/26270196.
Wang, C., Liu, H., Zhang, M., Wei, Z., 2018. The border effect on urban land expansion in China: The case of Beijing-Tianjin-Hebei region. Land. Use Policy 78, 287–294. https://doi.org/10.1016/j.landusepol.2018.06.050.
Wang, H., Guo, J., Zhang, B., Zeng, H., 2021. Simulating urban land growth by incorporating historical information into a cellular automata model. Landsc. Urban. Plan. 214, 104168. https://doi.org/10.1016/j.landurbplan.2021.104168.
Wang, H., Liu, Y., Zhang, G., Wang, Y., Zhao, J., 2021. Multi-scenario simulation of urban growth under integrated urban spatial planning: A case study of Wuhan, China. Sustain. (Switz.) 13 (20), 1–21. https://doi.org/10.3390/su132011279.
Wannewitz, M., Ajibade, I., Mach, K.J., Magnan, A., Petzold, J., Reckien, D., Ulibarri, N., Agopian, A., Chalastani, V.I., Hawxwell, T., Huynh, L.T.M., Kirchhoff, C.J., Miller, R., Musah-Surugu, J.I., Nagle Alverio, G., Nielsen, M., Nunbogu, A.M., Pentz, B., Reimuth, A., Garschagen, M., 2024. Progress and gaps in climate change adaptation in coastal cities across the globe. Nat. Cities 1 (9), 610–619. https://doi.org/10.1038/s44284-024-00106-9.
Wolff, C., Nikoletopoulos, T., Hinkel, J., Vafeidis, A.T., 2020. Future urban development exacerbates coastal exposure in the Mediterranean. Sci. Rep. 10 (1), 1–11. https://doi.org/10.1038/s41598-020-70928-9.
World Bank. (2020). Vietnam's Urbanization at a Crossroads: Embarking on an Efficient, Inclusive, and Resilient Pathway. https://doi.org/10.1596/34761.
Wu, H., Su, B., Jiang, T., Xu, R., Dong, Z., Huang, J., 2025. Projections of Urban Land Under the Shared Socioeconomic Pathways—A Case Study of Yangtze River Delta Region. Land 14 (10), 1995. https://doi.org/10.3390/land14101995.
Wu, X., Hu, Y., He, H., Xi, F., Bu, R., 2010. Study on forecast scenarios for simulation of future urban growth in Shenyang City based on SLEUTH model. Geo-Spat. Inf. Sci. 13, 32–39. https://doi.org/10.1007/s11806-010-0155-7.
Xiao, S., He, J., Yao, Y., Liang, X., Li, X., 2025. Optimizing urban three-dimensional landscapes in potential development areas to mitigate urban heat island effect under shared socioeconomic pathways. Landsc. Urban. Plan. 264, 105490. https://doi.org/10.1016/j.landurbplan.2025.105490.
Yang, L., Zhang, S., Yin, L., Zhang, B., 2022. Global occupation of wetland by artificial impervious surface area expansion and its impact on ecosystem service value for 2001–2018. Ecol. Indic. 142, 109307. https://doi.org/10.1016/j.ecolind.2022.109307.
Zhao, C., Jensen, J., Zhan, B., 2017. A comparison of urban growth and their influencing factors of two border cities: Laredo in the US and Nuevo Laredo in Mexico. Appl. Geogr. 79, 223–234. https://doi.org/10.1016/j.apgeog.2016.12.017.
Zhuang, H., Chen, G., Yan, Y., Li, B., Zeng, L., Ou, J., Liu, X., 2022. Simulation of urban land expansion in China at 30 m resolution through 2050 under shared socioeconomic pathways. GIScience & Remote. Sens. 59 (1), 1301–1320. https://doi.org/10.1080/15481603.2022.2110197.